Makorin 1 controls embryonic patterning by alleviating Bruno-mediated repression of *oskar* translation

Annabelle Dold[1]*, Hong Han[2]*, Niankun Liu[2]*, Andrea Hildebrandt[3,4], Mirko Brüggemann[5], Cornelia Rücklé[5], Anke Busch[6], Petra Beli[3], Kathi Zarnack[5], Julian König[4], Jean-Yves Roignant[1]^ and Paul Lasko[2]^

[1]RNA Epigenetics, Institute of Molecular Biology, 55128 Mainz, Germany. [2]Department of Biology, McGill University, Montréal, Québec, Canada H3G 0B1. [3]Chromatin Biology and Epigenetics, Institute of Molecular Biology, 55128 Mainz, Germany. [4]Genomic Views of Splicing Regulation, Institute of Molecular Biology, 55238 Mainz, Germany. [5]Buchmann Institute for Molecular Life Sciences, Frankfurt, Germany. [6]Bioinformatics Core Facility, Institute of Molecular Biology, 55128 Mainz, Germany.

*Equal contributions

^Corresponding authors: j.roignant@imb-mainz.de, paul.lasko@mcgill.ca

Keywords: Bruno, *oskar*, polyadenylation, oogenesis, germ cell specification, pole plasm, Mkrn1, *Drosophila*

Abstract

Makorins are evolutionary conserved proteins that contain C_3H-type zinc finger modules and a RING E3 ubiquitin ligase domain. In *Drosophila* maternal Makorin 1 (Mkrn1) has been linked to embryonic patterning and germ cell specification. Here, we show that Mkrn1 is required for translational activation of *oskar*, whose product is critical for axis specification and germ plasm assembly. We demonstrate that Mkrn1 interacts with poly(A) binding protein (pAbp) and binds *osk* 3' UTR in a region adjacent to A-rich sequences. This binding site also overlaps with Bruno (Bru) responsive elements (BREs), which regulate *osk* translation. We observe increased association of the translational repressor Bru with *osk* mRNA upon depletion of Mkrn1, implying that the two proteins compete for *osk* binding. Consistently, reducing Bru dosage partially rescues viability and Osk protein level in ovaries from *Mkrn1* females. We conclude that Mkrn1 controls embryonic patterning and germ cell formation by specifically activating *osk* translation via displacing Bru from its 3' UTR.

Introduction

In the *Drosophila* embryo, the maternally deposited pole plasm is a site of specialized translation of mRNAs required for germ cell specification and posterior patterning (Lasko, 2012). Numerous mRNAs accumulate in the pole plasm during oogenesis and early embryogenesis through several different localization mechanisms (Jambor *et al*, 2015; Lécuyer *et al*, 2007). Among these mRNAs is *oskar* (*osk*), which localizes to the posterior along a polarized microtubule network during oogenesis (Zimyanin *et al*, 2008). Several lines of evidence indicate that *osk* is the primary determinant that specifies germ cells and posterior patterning. Ectopic expression of *osk* at the anterior can induce a second set of anterior pole cells and a bicaudal embryonic segmentation pattern with mirror-image posterior segments (Ephrussi and Lehmann, 1992; Smith *et al*, 1992). In addition, mutations such as *Bicaudal-D* (*Bic-D*), *ik2*, and others that produce a duplicated anterior focus of *osk* mRNA also produce bicaudal embryos (Chang *et al*, 2011; Ephrussi *et al*, 1991; Shapiro and Anderson, 2006). Conversely, embryos from females carrying hypomorphic loss-of-function mutations of *osk* lack posterior segmentation and pole cells (Lehmann and Nüsslein-Volhard, 1986). Mutations in a number of other genes can produce a similar phenotype, and these are collectively known as posterior-group genes (Nüsslein-Volhard *et al*, 1987). Some of these genes (for example *cappuccino*, *chickadee*, *spire and staufen* (*stau*)) are required for posterior localization of *osk*. A failure to deploy *osk* produces the posterior-group phenotype (Manseau *et al*, 1996; Micklem *et al*, 2000). Other posterior-group genes (for example *vasa* (*vas*), *tudor*, *nanos* (*nos*), and *aubergine* (*aub*)), produce mRNAs and/or proteins that also accumulate in pole plasm and operate downstream of *osk* (Breitwieser *et al*, 1996; Lasko and Ashburner, 1990; Wang and Lehmann, 1991).

osk translation is under elaborate temporal and spatial regulation, ensuring that Osk protein becomes abundant only in the posterior pole plasm and not before stage 9 of oogenesis (Kim-Ha *et al*, 1995; Rongo *et al*, 1995; Markussen *et al*, 1995). A key repressor of *osk* translation prior to that stage and outside the pole plasm is Bruno (Bru), which interacts with binding sites called Bru response elements (BREs) in the *osk* 3' UTR. Mutations affecting the BREs result in earlier and excessive Osk expression (Kim-Ha *et al*, 1995; Webster *et al*, 1997). There is evidence for two distinct mechanisms of Bru-mediated repression: In the first, Bru recruits Cup, which inhibits assembly of an active cap-binding complex by competitive inhibition of eIF4G for binding to eIF4E (Nakamura *et al*, 2004). The second mechanism involves Bru-mediated oligomerization of *osk* mRNA into large particles that are inaccessible to the translational machinery (Chekulaeva *et al*, 2006).

While several proteins have been implicated in activating *osk* translation in the pole plasm (Wilson *et al*, 1996; Chang *et al*, 1999; Micklem *et al*, 2000), a comprehensive picture of how this is achieved has not yet emerged. For instance, it has been proposed that activation of *osk* translation involves inhibition of Bru (Kim *et al*, 2015). Related to this, a BRE-containing region in the distal part of the *osk* 3' UTR (BRE-C) functions in repression as well as in activation (Reveal *et al*, 2010). Nevertheless, the mechanism underlying the dual function of this element has not yet been solved.

Large-scale *in situ* hybridization screens have identified many other mRNAs that localize to the pole plasm (Lécuyer *et al*, 2007; Tomancak *et al*, 2007), and some of the corresponding genes could potentially also be involved in *osk* regulation. To search for new posterior-group genes, we previously expressed shRNAs targeting 51 different mRNAs that accumulate in the pole plasm. We observed that a substantial proportion

of embryos produced by *Makorin 1* (*Mkrn1*) knockdown females showed a posterior-group phenotype (Liu and Lasko, 2015). Makorin proteins are conserved in plants, fungi, and animals, and contain a RING-domain as well as one or more C_3H-type zinc fingers (ZnF) (Bohne *et al*, 2010). The role of these proteins is somewhat enigmatic despite their widespread evolutionary conservation. Mammalian MKRN1 has been identified as a E3 ubiquitin ligase that promotes degradation of target proteins (Kim *et al*, 2005), but proteomic analysis does not support an association with proteasome components (Carpenedo *et al*, 2016). MKRN1 has also been reported to interact with poly(A) binding protein (pAbp) and its shorter isoform stimulates translation in rat forebrain neurons (Cassar *et al*, Miroci *et al*, 2012).

Here, we analyzed the function of Mkrn1 during oogenesis and early embryogenesis. We generated several loss-of-function alleles that alter different domains of the *Mkrn1* coding sequence. We found that Mkrn1 is required for ensuring *osk* mRNA localization at the posterior pole, and for accumulation of Osk protein. Furthermore, we present evidence that Mkrn1 directly binds to a site in the *osk* 3'UTR that overlaps the BRE-C domain. This binding site is adjacent to an A-rich region that recruits pAbp to the 3'UTR (Vazquez-Pianzola *et al*, 2011). Moreover, the association between Mkrn1 and *osk* mRNA is stabilized by physical association with pAbp. Strikingly, depletion of *Mkrn1* results in an increased level of Bru binding to *osk* mRNA, and we observed precocious accumulation of Bru in *Mkrn1* mutant oocytes. Based on this evidence we propose that Mkrn1 competes with Bru for *osk* mRNA binding. In this manner it positively regulates *osk* translation, explaining the specific role of BRE-C in translational activation.

Results

The *Drosophila* genome includes four Makorin-related genes

In many organisms, up to four distinct genes encoding members of the Makorin family exist, but only one such gene, *Mkrn1*, has been annotated in *Drosophila*. To investigate whether flies are unusual in this regard, we used the protein basic local search alignment tool (BLASTP) to look for sequences similar to human MKRN1. This search uncovered four *Drosophila* genes, namely *Mkrn1, CG5334, CG5347,* and *CG12477*, with substantial similarity to *MKRN1* (Fig EV1A). All four predicted polypeptides from these genes contain a region of approximately 130 amino acids that is highly conserved and contains a RING-domain as well as C_3H-type zinc fingers (ZnF). The proteins are otherwise more divergent from one another, with the exception that all but CG12477 contain a ZnF domain near the amino-terminus. The four *Drosophila Makorin* genes do not obviously correspond one-by-one to their mammalian counterparts in terms of their sequence, since a BLASTP search with any of the four human MKRN proteins returns the same four *Drosophila* proteins in the same order (Mkrn1, CG5347, CG5334, CG12477, from greater to lesser similarity).

To analyze the differences in their functionalities, we first determined the expression profile of all four *Makorin* genes during development. *Mkrn1* mRNA is expressed at detectable levels at all developmental stages (Fig 1A) and clearly peaks in early (0 - 2.5 h) embryos and ovaries. In contrast, expression of the other three Makorin genes is undetectable during early development but rises in pupae and remains high in adult males, but not in females (Fig EV1B). Together, these results indicate that *Mkrn1* is the only gene of the family expressed in ovaries and early embryos and suggest that the three other genes could be specifically expressed in testes.

Mkrn1 mutants reveal essential roles in oogenesis and embryogenesis

To elucidate the role of *Mkrn1*, we used CRISPR/Cas9 to produce three different mutant alleles: $Mkrn1^{N}$, a complete deletion of the coding sequence, $Mkrn1^{S}$, a frameshift mutation that is predicted to produce a C-terminally truncated protein of 124 amino acids, including only ZnF1 among conserved domains, and $Mkrn1^{W}$, a small in-frame deletion that disrupts only the ZnF1 domain (Fig 1B). In the strong *Mkrn1* mutants ($Mkrn1^{S}$ *and* $Mkrn1^{N}$), most egg chambers cease development at or before stage 10 (Figs 1C-J). Most oocytes from $Mkrn1^{S}$ mutants that progress as far as stage 9 or later display an oocyte nucleus that remained at the posterior and failed to migrate to the antero-dorsal corner (Fig 1M). The very few eggs laid by $Mkrn1^{S}$ females have no dorsal appendages and do not develop (Fig 1Q). $Mkrn1^{N}$ egg chambers did not progress as far as stage 9 and showed variable defects in early oogenesis including failure of oocyte differentiation (Fig 1N) and inappropriate follicle cell migration (Figs 1J and N). On the other hand, ovaries of females homozygous for $Mkrn1^{W}$ have a similar morphology to wild-type (Figs 1C and D). $Mkrn1^{W}$ mutant ovaries completed oogenesis and produced fertilizable eggs in similar numbers as wild-type controls (Figs 1G, H, K and L, and Table EV1). However, most embryos produced by $Mkrn1^{W}$ females (subsequently called $Mkrn1^{W}$ embryos) lacked posterior segments and pole cells (Figs 1O-P, and EV2A), a phenotype similar to *osk* mutants and to what we previously observed at lower frequency from females expressing shRNA targeting *Mkrn1* (Liu and Lasko, 2015). However, the few eggs produced by $Mkrn1^{W}$ females that hatched (40/1222, 3.3%, Table EV1) can complete development to adulthood.

To determine whether these Mkrn1 functions were specific to the germline and/or to the follicle cells we produced flies in which only the germline was mutant for $Mkrn1^{N}$, using the FLP-dominant female sterile technique (Chou and Perrimon, 1996). The ovaries from these flies appeared very similar to those from $Mkrn1^{N}$ homozygotes (Fig

EV2B). In contrast, driving shRNA targeting *Mkrn1* in follicle cells with the T155 driver (Hrdlicka *et al*, 2002) gave no phenotype (Fig EV2C). Moreover, $Mkrn1^{S}$, $Mkrn1^{W}$, and $Mkrn1^{N}$ females could be rescued to fertility by *nos>GAL4* driven germline expression of transgenes encoding *Mkrn1* tagged by either FLAG or Venus (Table EV1). Taken together, these results indicate that germline expression of *Mkrn1* is essential for completion of oogenesis, posterior embryonic patterning and pole cell specification.

Mkrn1 accumulates in pole plasm during oogenesis

To examine the distribution of Mkrn1 in the germline, we expressed Venus- and FLAG-tagged Mkrn1 using the *nos>GAL4* driver. Since *Mkrn1* females could be rescued to fertility by germline specific expression of these transgenes (Table EV1), we concluded that these tagged transgenes are functional, and thus inferred that their localization should reflect the endogenous one. As we obtained similar results for both tagged forms, for simplicity we will refer to them here as Mkrn1 but identify the specific tag in the accompanying figures. When overexpressed in ovaries, Mkrn1 becomes detectable in a uniform distribution in germline cells from early oogenesis. We observed a mild accumulation of Mkrn1 in cytoplasmic particles resembling nuage at the outer surface of nurse cell nuclear membranes and in the early oocyte (Fig 2A, and Figs EV3A and S). In later egg chambers Mkrn1 remains abundant in nurse cells but tightly localized in the pole plasm in the oocyte (Fig 2D). Next, we conducted double labelling experiments in wild-type ovaries to determine the degree of colocalization between Mkrn1 and known pole plasm components. In both stage 8 and stage 10 oocytes, Mkrn1 co-localizes extensively with Stau (Figs 2A-F, and EV3A-F), *osk* mRNA (Figs 2G-L), Osk protein (Figs EV3G-L), Vas (Figs EV3M-R) and Aub (Figs EV3S-X). This close

association between Mkrn1 and many important pole plasm components suggests that Mkrn1 is an integral component of pole plasm.

To determine whether Mkrn1 depends on the pole plasm assembly pathway (Mahowald 2001) for its posterior localization, we expressed the tagged *Mkrn1* transgenes in *osk* and *vas* mutant backgrounds. We found that loss of *osk* abolished Mkrn1 localization (Figs 2M and N, and EV4A). In contrast, Mkrn1 localized normally to the posterior in *vas* mutant oocytes (Figs 2O and P, and EV4B), placing Mkrn1 between *osk* and Vas in the pole plasm assembly pathway.

Mkrn1 ensures correct localization of specific mRNAs and proteins involved in embryonic patterning

To obtain insights into the link between Mkrn1 and pole cell determination, we collected embryos from females trans-heterozygous for a *Mkrn1* allele and for either a *vas* or *osk* allele. Next, we compared the number of pole cells with single heterozygous controls. When heterozygous, $Mkrn1^{W}$ or $Mkrn1^{S}$ had little effect on pole cell number. However, either allele reduced the number of pole cells produced by vas^{PH} heterozygotes, and further by osk^{54} heterozygotes (Fig EV5A). These data support a genetic interaction between *Mkrn1* and genes involved in embryonic patterning and pole cell specification.

To address whether mutations of the *Mkrn1* gene may affect the distribution of proteins involved in embryonic patterning we performed immunostaining experiments. Strikingly, we found that Osk protein did not accumulate at the posterior pole of the oocyte in all *Mkrn1* alleles and that its level appeared reduced (Figs 3A-D). For Stau we observed weaker and more diffuse posterior localization in $Mkrn1^{W}$ as compared to

wild-type (Figs 3E and F, and EV5B-D) and little detectable protein in *Mkrn1*^{S} and *Mkrn1*^{N} (Figs 3G and H). On the other hand, Grk localized normally to the antero-dorsal corner of the oocyte in *Mkrn1*^{W} (Figs 3I and J, and EV5E-G). In *Mkrn1*^{S}, Grk was observed at reduced levels associated at the posterior with the mislocalized oocyte nucleus (Fig 3K, and EV5H-J) and diffusely distributed at a very low level in *Mkrn1*^{N} (Fig 3L). Posterior localization of Aub and Vas was lost in oocytes of all *Mkrn1* mutant alleles (Figs 3M-T). Finally, Orb localization was unaffected in *Mkrn1*^{W} (Figs 3U and V), but was concentrated at the posterior in *Mkrn1*^{S} (Fig 3W). Many *Mkrn1*^{N} egg chambers included a single Orb-positive cell (Fig 3X), indicating that in these cases oocyte differentiation had taken place. Importantly, normal accumulation of all proteins could be restored by *nos*>GAL4 driven expression of a tagged *Mkrn1* transgene (Fig EV6), confirming the specificity of the *Mkrn1* phenotypes.

Next, we used fluorescent *in situ* hybridization to investigate the distribution of several mRNAs involved in patterning in *Mkrn1*^{W} and *Mkrn1*^{S} oocytes, and in *Mkrn1*^{W} embryos. Consistent with what we observed for Grk protein, localization of *grk* mRNA was similar to wild-type in *Mkrn1*^{W}, but remained at the posterior in *Mkrn1*^{S} oocytes (Figs 4A-C). Localization of *osk* mRNA to the early oocyte was normal in *Mkrn1*^{W} and *Mkrn1*^{S}, but its localization to the pole plasm was incomplete in most egg chambers (*Mkrn1*^{W}) or absent (*Mkrn1*^{S}) (Figs 4D-F). Posterior *osk* accumulation was also lost in some *Mkrn1*^{W} embryos (Figs EV7A and B), as was that of *nos* and *polar granule component* (*pgc*) mRNAs (Figs EV7C-F). We conclude from these experiments that Mkrn1 is essential for *osk* mRNA localization to the pole plasm and thus for all subsequent stages of pole plasm assembly.

To further examine the effects of *Mkrn1* mutations on Osk expression in ovaries, we compared Osk protein levels by western blot analysis and *osk* mRNA levels by quantitative PCR. Strikingly, we observed a pronounced reduction in Osk protein (Fig 4G), but not of *osk* mRNA (Fig 4H), in all *Mkrn1* alleles. These results imply that *Mkrn1* contributes to post-transcriptional regulation of *osk*.

Mkrn1 physically associates with factors involved in *osk* mRNA localization and translation

To gain further insights into the molecular pathways underlying Mkrn1 function we sought to identify potential cofactors. For this purpose, we expressed Myc-tagged Mkrn1 in *Drosophila* S2R+ cultured cells and carried out immunoprecipitation (IP) experiments followed by mass-spectrometry analysis. We also repeated this experiment using a version of Mkrn1 carrying a point mutation in the RING domain, as we noticed that this construct was expressed at a much higher level compared to the wildtype one, which appears to be unstable after transfection in the cells (Figs EV8A and B). Similar stability characteristics have also been reported for mammalian MKRN1 (Kim *et al*, 2005). Interestingly, numerous RNA-binding proteins were enriched after IP, in particular when using Mkrn1^{RING} as bait (Figs EV8C and D). Among those, several have been already linked to *osk* mRNA localization and translation (Nakamura *et al*, 2001; Nakamura *et al*, 2004; Norvell *et al*, 2005; Steinhauer and Kalderon, 2005; Vazquez-Pianzola *et al*, 2011). To validate these interactions and address whether an RNA intermediate was involved, we performed co-IP experiments in S2R+ cells with Mkrn1^{RING} and various interaction partners in the presence or absence of RNase T1. Using this approach, we could confirm interaction with poly(A) binding protein (pAbp), IGF-II mRNA-binding protein (Imp), eukaryotic initiation factor 4G (eIF4G), Squid (Sqd) and maternal expression at 31B (me31B), all in an RNA-independent manner

(Fig EV9). Interestingly, several of these components have previously been shown to interact with each other (Nakamura *et al*, 2001; Norvell *et al*, 2005; Geng and Macdonald, 2006; Clouse *et al*, 2008; McDermott *et al*, 2012). We further confirmed that these interactions occur *in vivo* between FLAG-tagged Mkrn1 and pAbp as well as eIF4G (Fig 5A and Fig EV9F).

To further address the strength of these interactions, co-IPs were repeated in a variety of salt concentrations. We found that pAbp and eIF4G interact most strongly with Mkrn1 and these interactions were maintained upon stringent washes (Figs 5B and EV10). Consistent with this result, the stability of Mkrn1 itself was strongly enhanced upon co-transfection of pAbp (Fig 5C). Mammalian MKRN1 contains a PCI/PINT associated module 2 (PAM2) motif, that is present in several pAbp binding proteins and serves in vertebrate MKRN1 for binding to PABP (Miroci *et al*, 2012). We identified a similar motif in *Drosophila* Mkrn1 (Fig 5D), but with one variation compared to human (V instead of E at position 9) that likely explains why this PAM2 motif was not recognized previously. To address the functionality of this motif we produced a mutant version (Mkrn1^{PAM2}, Fig 5D), repeated the co-IPs, and found that when this domain was mutated the interaction between Mkrn1 and pAbp was compromised (Fig 5E). Based on these data we conclude that Mkrn1 exists in one or several complexes that contain factors involved in the regulation of *osk* mRNA localization and translation, and stably interacts with pAbp via its PAM2 motif.

Mkrn1 associates specifically with *osk* mRNA *in vitro* and *in vivo*

The mislocalization of *osk* and *grk* mRNAs in *Mkrn1* ovaries prompted us to test whether Mkrn1 can interact with these mRNAs. To assess whether Mkrn1 can bind RNA, we immunoprecipitated FLAG-Mkrn1 after transfection in S2R+ cells and UV

crosslinking. Mkrn1-bound RNA was subsequently labeled, and protein-RNA complexes were visualized by autoradiography (Fig EV11A). While a higher concentration of RNase I (1/50 dilution) resulted in a focused band, a lower concentration (1/5000 dilution) produced a shift of the Mkrn1-RNA complexes, demonstrating the RNA binding ability of *Drosophila* Mkrn1. We next repeated this experiment with various mutations in different Mkrn1 domains (Fig EV8A). While mutations that alter the RING (Mkrn1^{RING}) or the ZnF2 domain (Mkrn1^{ZnF2}) behave as wild-type Mkrn1, deletion of the ZnF1 domain (Mkrn1$^{\Delta ZnF1}$) resulted in a reduction of labeled Mkrn1-RNA complexes. These findings demonstrate that the ZnF1 domain is critical for association of Mkrn1 with RNA (Fig EV11A).

To address whether Mkrn1 associates with specific mRNAs *in vivo* we overexpressed either wild-type Mkrn1 or Mkrn1$^{\Delta ZnF1}$ in ovaries and performed RNA IP (RIP) experiments. The enrichment of different mRNAs was analyzed by qPCR using primers that bind to 3'UTRs of different transcripts. We chose to analyze the 3'UTRs as these regions are often of importance for regulating mRNA. We observed that *osk* mRNA was substantially enriched in Mkrn1 IPs, but much less when using Mkrn1$^{\Delta ZnF1}$ (Fig 6A). On the other hand, *bcd* and *grk* mRNAs were not detected above background levels in either RIP experiment (Figs 6A, and EV11B). This provides evidence that Mkrn1 binds specifically to *osk* mRNA *in vivo* and that its ZnF1 domain is important for this interaction.

To further determine precisely where Mkrn1 binds *osk* mRNA, we performed crosslinking and IP (iCLIP) experiments after transfection of a tagged *Mkrn1* construct in S2R+ cells (Fig EV11C). Since *osk* is poorly expressed in these cells we co-transfected a genomic construct of *osk* under the control of an *actin* promoter. We found

many Mkrn1 peaks in ribosomal RNA genes, with no specific distribution with respect to their sequences. However, we also observed specific binding sites in the distal part of the *osk* 3' UTR (Fig 6B). These sites fall just upstream of A-rich sequences that recruit pAbp (Vazquez-Pianzola *et al*, 2011). Moreover, the binding site of Mkrn1 overlaps with the BRE-C, which is bound by Bru and is required for both repression and activation of *osk* translation (Reveal *et al*, 2010). To validate the identified Mkrn1 binding sites we performed RIP experiments in S2R+ cells using different versions of *osk* 3' UTR fused to the firefly luciferase coding sequence. We found that Mkrn1 binds strongly to *osk* 3'UTR but only weakly to *grk* 3'UTR (Fig EV12A). In contrast, deletion of the Mkrn1-bound sites identified with iCLIP ($osk^{\Delta Mkrn1}$) greatly reduced the interaction of Mkrn1 to *osk* 3' UTR (Figs 6C, and EV12B).

As the Mkrn1 binding sites lie just upstream of the A-rich region (AR) we wondered whether the AR would also have an impact on Mkrn1 binding. To test this possibility, we deleted the AR ($osk^{\Delta AR}$), and examined Mkrn1 binding. We observed a decrease of Mkrn1 binding similar to that observed when deleting the Mkrn1 binding sites (Figs 6D, and EV12C). Thus, we conclude that the AR enhances Mkrn1 binding to *osk* 3' UTR. As Mkrn1 forms a stable complex with pAbp, our results further suggest that pAbp binding to the AR stabilizes Mkrn1 and therefore enhances its interaction with *osk*. Accordingly, reducing pAbp levels by RNAi, but not the level of Imp, another Mkrn1 interactor, dramatically decreased Mkrn1 association with *osk* mRNA (Figs 6E, and EV12D and E). Mutation of the PAM2 domain that enables the interaction with pAbp also resulted in reduced binding to *osk* 3'UTR (Figs 6F, and EV12F). Consistent with these results, mutating both the ZnF1 domain and the PAM2 motif led to almost complete loss of binding to *osk* 3'UTR. Collectively, our results indicate that Mkrn1

binds specifically to the 3' end of *osk* 3'UTR via its ZnF1 domain and this association is further stabilized through the interaction with pAbp via the PAM2 motif.

Mkrn1 competes with Bru for binding to *osk* 3'UTR

Our observation that Mkrn1 binds to the BRE-C prompted us to test whether Mkrn1 and Bru may compete for binding to *osk* 3'UTR. To this end, we first examined whether we can recapitulate Bru binding to *osk* mRNA in S2R+ cells. As Bru is normally not expressed in this cell type, cells were co-transfected with a *Bru* construct tagged with GFP along with the *luciferase-osk*-3'UTR reporter. RIP experiments were performed and confirmed previous findings that Bru strongly binds to *osk* 3' UTR (Fig EV13A; Kim-Ha *et al*, 1995). We next repeated this experiment upon knockdown of *Mkrn1* mRNA. Strikingly, while the overall level of Bru was not affected (Fig EV13B), its binding to *osk* 3'UTR was significantly increased (Figs 7A and EV13B and C). As pAbp is required to stabilize Mkrn1 binding to *osk* 3'UTR, we wondered whether this interaction is necessary for modulating Bru binding. Indeed, knockdown of pAbp resulted in an increase in Bru binding to *osk* 3'UTR (Figs 7B and EV13D). To assess whether Mkrn1 competes with Bru for binding to the *osk* 3'UTR *in vivo*, we repeated RIP experiments using ovarian extracts. Bru binding was assessed using an antibody directed against endogenous Bru and its association with *osk* mRNA was subsequently analyzed by qPCR. Similar to S2R+ cells, Bru binding to *osk* 3'UTR was significantly increased in $Mkrn1^{W}$ mutant ovaries (Figs 7C, and EV13E). Thus, we conclude that Mkrn1 restricts Bru binding to *osk* 3'UTR and this effect is enhanced by the interaction of Mkrn1 with pAbp.

To further address the relationship between Mkrn1 and Bru we examined whether the $Mkrn1^{W}$ mutation affects Bru accumulation during oogenesis. In wild-type ovaries, Bru

is expressed in all germline cells and accumulates to a modest degree in the oocyte during early oogenesis, (Figs 7D and E; Webster *et al*, 1997). In contrast, in *Mkrn1*^{W} ovaries, oocyte accumulation of Bru during early stages was much more pronounced (Figs 7F and G). As *osk* mRNA accumulates in early oocytes, this is consistent with Bru having an increased binding affinity for *osk* in the absence of Mkrn1. In stage 10 wild-type oocytes, there is faint accumulation of Bru in the pole plasm (Figs EV13F-K; Webster *et al*, 1997). In similarly staged *Mkrn1*^{W} oocytes, Bru continued to co-localize with *osk* RNA even when posterior accumulation of *osk* was perturbed (Figs EV13L-Q).

If Mkrn1 activates *osk* translation solely by displacing Bru, we would predict that lowering *Bru* genetic dosage should suppress the *Mkrn1* phenotype. To test this hypothesis, we used the strong *Bru* allele (*bru1*^{QB}) and performed genetic experiments with the *Mkrn1*^{W} allele (Schüpbach and Wieschaus 1991; Webster *et al*, 1997). Indeed, removing one copy of *Bru* was sufficient to partially rescue Osk protein level in *Mkrn1*^{W} female oocytes as measured by immunostainings (Figs 7H-M). We also observed a substantially higher survival rate of embryos produced from *Mkrn1*^{W} females that were heterozygous for *bru1* as compared to controls (620/2058, 30.1% vs 40/1222; 3.3%). Taken together, these experiments support a model in which Mkrn1 activates *osk* translation by displacing Bru binding to the *osk* 3'UTR (Fig 7N).

Discussion

Our data indicates that Mkrn1 is essential for embryonic patterning and germ cell specification. By taking advantage of a new allele that specifically disrupts Mkrn1 binding to RNA we demonstrate that Mkrn1 exerts this function primarily via regulating *osk* translation by antagonizing Bru binding.

Control of *osk* translation has been studied in depth, revealing a complex spatio-temporal interplay between repressing and activating factors (Lehmann 2016). A key factor in translational repression is Bru, which binds to the *osk* 3'UTR and acts in early-stage oocytes as well as outside of the pole plasm in later-stage oocytes (Kim-Ha *et al*, 1995; Markussen *et al*, 1995; Rongo *et al*, 1995). Translational repression by Bru occurs via recruitment of Cup, an eIF4E-binding protein that is a competitive inhibitor of eIF4G (Wilhelm *et al*, 2003; Nakamura *et al*, 2004). Bru can also oligomerize RNAs such as *osk* that contain multiple Bru binding sites, rendering them inaccessible to ribosomes (Chekulaeva *et al*, 2006; Besse *et al*, 2009; Kim *et al*, 2015). However, less is known about how *osk* repression by Bru is relieved and its translation is activated in the pole plasm. This process is likely to involve multiple redundant mechanisms. For example, Bru can be phosphorylated on several residues, and phosphomimetic mutations in these residues inhibit Cup binding in pulldown assays; but these changes do not seem to affect translational repression activity *in vivo* (Kim *et al*, 2015). In agreement with this, we did not observe a change in Bru binding to itself nor to Cup upon depletion of Mkrn1 (Figs EV14A and B). Stau, Aub, Orb and pAbp have also been implicated in activating *osk* translation (Wilson *et al*, 1996; Micklem *et al*, 2000; Castagnetti and Ephrussi 2003; Vazquez-Pianzola *et al*, 2012). It is unlikely that Mkrn1 controls *osk* translation by recruiting Stau as Stau still colocalizes with *osk* mRNA in $Mkrn1^{W}$ oocytes (Figs EV13Q-S). Instead, we propose that Mkrn1 exerts its positive

activity at least in part by competing with Bru binding on *osk* mRNA. This is evidenced by the overlap of their binding sites, the increased Bru binding upon Mkrn1 knockdown and by the fact that reducing *bru1* dosage is sufficient to partially alleviate *osk* translational repression.

Two distinct Bru binding regions (AB and C) are present in the *osk* 3' UTR and are required for translational repression. However, the C region has an additional function in translational activation. Indeed, it was hypothesized that an activator may bind the C region to relieve Bru-mediated repression (Reveal *et al*, 2010). Later work showed that Bicoid Stability Factor (BSF) binds the C region *in vitro*, precisely where we mapped Mkrn1 binding (3' type II site) (Ryu and Macdonald 2015). Deletion of this site impacts embryonic patterning, yet depletion of BSF has no effect on Osk protein expression up to stage 10, indicating that initial activation of *osk* translation is effective even in the absence of BSF. In this case, only late stage oocytes display reduced Osk accumulation. Therefore, it is possible that a concerted action of Mkrn1 and BSF exists at the type II site to trigger *osk* translation and sustain it at later stages.

One remaining mystery is the dynamic of the interplay between Bru and Mkrn1. Mkrn1 colocalizes with *osk* mRNA before it completes its transport to the pole plasm (Fig EV3). Therefore, why then Mkrn1 does not release the repression by Bru before reaching the posterior pole? In fact, we do observe increased Bru staining in early egg chambers devoid of Mkrn1 (Figs 7F and G), suggesting that competition between Mkrn1 and Bru for binding to *osk* already exists at early stages. Perhaps there are redundant mechanisms that ensure *osk* repression during its transport despite reduced association of Bru with *osk* mRNA when Mkrn1 is present. A second possibility is that Mkrn1 exerts an additional function once reaching the posterior pole that enables *osk*

translation. pAbp accumulates at the posterior pole of stage-10 oocytes (Vazquez-Pianzola *et al*, 2011), and previous studies indicate that translational activation of *osk* in the pole plasm involves lengthening of its poly(A) tail (Chang *et al*, 1999; Castagnetti and Ephrussi 2003). Therefore, it is possible that higher local concentration of pAbp in the pole plasm leads to better recruitment of Mkrn1 to *osk* RNA and consequent displacement of Bru. There also may be additional functions of Mkrn1 with respect to *osk* translation, perhaps depending on its E3 ligase activity. We have not obtained evidence for Bru ubiquitylation by Mkrn1 (Fig EV14C) but an indirect mechanism cannot be ruled out.

The binding of Mkrn1 to *osk* mRNA seems to be extremely specific as we did not recover any other mRNA to a comparable extent in any RIP or iCLIP experiments that we performed. We found that this binding is dependent on a downstream A-rich sequence and on interaction with pAbp. Relevant to this, Bru binds to *grk* RNA in addition to *osk* (Filardo and Ephrussi, 2003; Reveal *et al*, 2011), and several proteins that associate with Mkrn1 also associate with *grk* (Geng and Macdonald 2006; Clouse *et al*, 2008). However, we found that Mkrn1 does not bind strongly to *grk*, which lacks poly(A) stretches in the proximity of its Bru binding sites, and consistently, Mkrn1 does not regulate *grk* translation.

In addition to pAbp, it is noteworthy that Mkrn1 associates with other proteins previously implicated in *osk* localization and translational activation. Its interaction with eIF4G would be consistent with a role in alleviating Cup-mediated repression, as it could recruit eIF4G to the cap-binding complex at the expense of Cup. However, we did not observe an interaction between Mkrn1 and eIF4E (Appendix Tables S1 and S2). The association between Mkrn1 and Imp is also intriguing as *osk* 3'UTR contains 13

copies of a five-nucleotide motif that binds to Imp. These motifs are essential for translation and posterior anchoring although Imp itself is not (Munro *et al*, 2006). In contrast to pAbp, we did not observe alteration of Mkrn1 binding when Imp was depleted, indicating that Imp is not required to stabilize Mkrn1 on *osk* mRNA.

The molecular links we uncovered between Mkrn1 and RNA-dependent processes in *Drosophila* are consistent with recent high-throughput analysis of mammalian MKRN1 interacting proteins (Cassar *et al*, 2015). RNA binding proteins, including PABPC1, PABPC4, and eIF4G1, were highly enriched among the interactors. In the same study MKRN1 was also shown to interact with RNA. In addition, the short isoform of rat MKRN1 was shown to activate translation (Miroci *et al*, 2012). Since in vertebrates *MKRN* genes are also highly expressed in gonads and early embryos, it is possible that similar molecular mechanisms are employed to regulate gene expression at these stages (Bohne *et al*, 2010). Along these lines, MKRN2 was found recently to be essential for male fertility in mice (Qian *et al*, 2016). Thus, our study provides a solid framework for future investigations deciphering the role of vertebrates MKRN in post-transcriptional control of gene expression during gametogenesis and early development.

Materials and Methods

Generation of *Mkrn1* mutants using CRISPR/Cas9

The guide RNAs used were cloned into expression vector pDFD3-dU63gRNA (Addgene) according to manufacturer's instructions. Different guide RNAs were used either alone (gRNA1 starting at nucleotide 64 of *Mkrn1* CDS and gRNA2 starting at nucleotide 363 of *Mkrn1* CDS) or in combination (gRNA3 starting at nucleotide 387

of *Mkrn1* gene and gRNA4 starting at nucleotide 2239). *vas*-Cas9 *Drosophila* embryos were injected with the purified plasmids containing the gRNA (500 ng/µl in H_2O) and allowed to develop to adulthood. Each male was crossed with double balancer females. Genomic PCR from single flies was prepared and tested for CRISPR/ Cas9 induced mutations using the T7 endo I (BioLabs) assay or by PCR using primers that bind in proximity to the guide RNA targeting site. A list of gRNAs as well as primers is appended (Appendix Table S3).

Immunostaining and confocal imaging:

Ovaries were dissected and fixed in 4% paraformaldehyde in PBS for 20 min at room temperature (RT). After 4-5 washes in PBST (PBS containing 0.3% Triton-X100) ovaries were permeabilized with 1% freshly prepared Triton-X100 in PBS for 1 h. The ovaries were blocked in 2% BSA/PBST overnight. Dispersed egg chambers were then incubated with the primary antibodies diluted in 2% BSA/PBST at RT for 4 h or overnight at 4°C. The washed egg chambers were incubated with conjugated secondary antibodies at 1:500 at RT for 4 h or overnight at 4°C. DAPI (1 ng/ml) was added in the last wash to counter-stain the nuclei for 30 min. After 2-3 washes with PBST the mounting medium containing 1% DABCO was added and the samples were equilibrated for 30 min or overnight. The stained samples were mounted on glass slides and sealed with nail varnish for microscopy imaging. Rabbit polyclonal antibodies against Vas, Osk, Aub, Grk were generated in the Lasko lab; rabbit α-Stau is a gift from the St Johnston lab; rabbit α-Bru is from the Ephrussi lab and rabbit α-pAbp is from the Sonenberg lab; mouse monoclonal antibodies against Orb, Sqd, and Lamin were purchased from the Developmental Studies Hybridoma Bank; mouse α-GFP and rabbit α-Flag were purchased from Abcam and Sigma. Alexa Fluor 488 or 555 conjugated secondary antibodies were purchased from Molecular Probes, and pre-absorbed with

fixed and blocked wild type ovaries to reduce background. Stained egg chambers were examined using a confocal microscope (Leica). Images were taken under 40 x oil lens by laser scanning and processed with ImageJ.

In situ hybridization of embryos and ovaries and RNA-protein double labeling

cDNAs were used as templates for PCR to generate an amplified gene fragment with promoter sequences on each end. PCR products were purified via agarose gel extraction and used for *in vitro* transcription to generate digoxigenin-labeled RNA antisense probes with MAXIscript kit (Ambion). The length of each probe was about 1000 nt. *In situ* hybridization experiments were performed as described (Lécuyer *et al*, 2008), using biotinylated α-DIG antibody and streptavidin-HRP followed by tyramide conjugation for development of FISH signal. For RNA-protein double labeling, ovaries or embryos were incubated in primary antibody against the protein of interest along with biotinylated α-DIG antibody at 4°C overnight. The tissue was washed, then detection reagent (fluorochrome-conjugated secondary antibody) along with streptavidin-HRP was added and incubated at 4°C overnight. Images were taken with confocal microscope (Leica).

Embryo cuticle preparation and staining

Flies were transferred into egg-laying cages with apple juice agar plates and incubated at 25°C in the dark. Embryos were collected when 50-100 eggs had been laid and allowed to age for 24 h at 25°C. Embryos were collected in a sieve, dechorionated with 50% bleach for 2.5 min, washed with water, then transferred into PBST buffer (PBS + 0.1% Tween 20). For cuticle preparations, PBST buffer was removed, then 40-50 µl of Hoyer's solution was added and embryos were kept at 4 °C overnight. Embryos in Hoyer's solution were mounted on a glass slide, covered with a cover slip

and incubated at 60-65 °C overnight. Dark-field images were taken; with Leica DM6000B microscope.

Staging

Staging experiment was performed as described (Lence *et al*, 2016) using *D. melanogaster* w^{1118} flies.

Cell line

Drosophila S2R+ are embryonic derived cells obtained from Drosophila Genomics Resource Center (DGRC, Flybase ID: FBtc0000150).

Cell culture, RNAi, transfection

Drosophila S2R+ cells were grown in Schneider's medium (Gibco) supplemented with 10% FBS (Sigma) and 1% Penicillin-Streptomycin (Sigma). For RNAi experiments, PCR templates for the dsRNA were prepared using T7 Megascript Kit (NEB). S2R+ cells were seeded at the density of 10^6 cells/ml in serum-free medium and 15 µg/ml of dsRNA was added to the cells. After 6 h of cell starvation, serum supplemented medium was added to the cells. dsRNA treatment was repeated after 48 h and cells were collected 24 h after the last treatment. A list of primers used to create dsRNA templates by PCR is appended (Appendix Table S4). Effectene (Qiagen) was used to transfect vector constructs in all overexpression experiments following the manufacturer's protocol.

Immunoprecipitations (IPs)

For IP experiments in S2R+ cultured cells, protocol was followed as described (Lence *et al*, 2016) with minor changes: 2 mg of the protein lysates was incubated for 2 h with

10 µl of either Myc-Trap® or GFP-Trap® beads (Chromotek). To determine the dependence of interactions on RNA, 50 U of RNaseT1 (ThermoFisher) were added to the respective IP. To ensure the activity of RNase T1, lysates were incubated 10 min at RT prior to the incubation of lysate with antibody. For IP experiments in ovaries, 150 µl of wet ovaries from 3-5 day old flies expressing Venus-Mkrn1 was homogenized on ice in 2 ml of cold IP buffer (1 X PBS, 0.4% Triton X-100, 1 mM $MgCl_2$, 5% glycerol), containing protease inhibitors and PMSF. The extracts were diluted to 1.5 mg protein/ml. Each extract (0.66 ml) was mixed with 24 µg of anti-pAbp Fab antibody (Smibert lab; Na *et al*, 2016), 17 µg of α-eIF4G rabbit antibody, or 15 µl of rabbit anti-α–Tubulin antibody (Abcam). When present, 100 µg RNase A (Qiagen) was added to the samples. Samples were incubated with rotation at 4 °C overnight, then mixed with 30 µl of protein A agarose beads (wet volume, Invitrogen) and incubated with rotation at RT for 1.5 h. The beads were washed three times with IP buffer. Bound material on the beads was eluted by boiling for 2 min in 40 µl of SDS loading buffer. 20 µl of the eluted sample, together with input samples, was used for western blot.

RNA- Immunoprecipitation (RIP)

For RIP, S2R+ cells or ovaries were harvested and lysed in RIP buffer (150 mM NaCl, 50 mM Tris-HCl pH 7.5, 0.5% NP-40, 1 mM EDTA) supplemented with proteinase inhibitors (1.5 µg/ml Leupeptin, 1.5 µg/ml Pepstatin, 1.5 µg/ml Aprotinin and 1.5 mM PMSF) and RNase inhibitors (20 U/µl). S2R+ cells were lysed for 20 min at 4°C, subtracted to 2 cycles of sonication on a bioruptor (Diagenode) with 30 sec "ON"/"OFF" at low setting and the remaining cell debris was removed by centrifugation at 21,000 g for 10 min at 4°C. To remove lipids and cell debris, ovary lysates were centrifuged 4 times. Protein concentrations were determined using Bradford reagent (BioRad). 2 mg of protein lysate were incubated for 3 h with 2 µg of α-FLAG M2® antibody (Sigma-

Aldrich) pre-coupled to 20 µl of rotein G Dynabeads® (Thermo Fisher Scientific) head-over-tail at 4°C. For RIP experiments analysing binding of Bru in ovaries, either 1 µl of rabbit α-Bru (gift from A. Ephrussi) or 2 µg of rabbit IgG (Millipore) were incubated with ovarian lysate over night at 4°C. 20 µl of protein G Dynabeads® were added for 2 h after the incubation. For every RIP experiment, beads were washed 4 x for 10 min in RIP buffer at 4°C. For immunoprecipitation of GFP-tagged Imp and Bru 15 µl of GFP-Trap® (Chromotek) were used. Lysates were prepared similar as above using RIPA buffer (140 mM NaCl, 50 mM Tris pH 7.5, 1 mM EDTA pH 8, 1% Triton X-100, 0.1% SDS, 0.1% sodium deoxycholate) supplemented with proteinase and RNase inhibitors. IP was performed for 2 h at 4°C and subsequently washed 4 x for 10 min with RIPA buffer. RNA was eluted in TRIzol Reagent (ThermoFisher), 10 min at RT and subjected to RNA isolation and RT-qPCR. To obtain the depicted fold enrichment, individual transcripts were normalized to either *18S* or *rpl15*. Al least three biological replicates were performed for each experiment. Statistical analysis was performed using paired t-test. To analyze IP, 30% of beads were eluted in 1x SDS buffer (50 mM Tris pH 6.8, 2% SDS, 10% glycerol, 100 mM DTT, 0.05% Bromphenol Blue) at 95°C for 10 min. Eluted IP proteins were removed from the beads and analyzed by western blot together with input samples.

Western blotting

Western blotting was performed as described (Lence *et al*, 2016). Primary antibodies used were: mouse α-Myc 9E10 antibody (1:2000, Enzo Life Sciences); mouse α-FLAG M2® antibody (1:1000, Sigma-Aldrich); rabbit α-GFP TP401 antibody (1:5000, Acris Antibodies); mouse α-HA F7 (1:1000, Santa-Cruz) rat α-HA (1:750, Roche); mouse α-β-Tubulin (1:5000, Covance), mouse α-α-Tubulin (1:20,000; Sigma), mouse α-GFP (1:500; Molecular probe), mouse α-ubiquitin (1:1.000; Santa Cruz) Fab α-

pAbp (2.5 µg in 5 ml), α-eIF4G rabbit antibody (1 µg in 5 ml), rabbit α-Osk (1:1000) antibody was a gift from A. Ephrussi.

RNA isolation and measurement of RNA levels

Cells or tissues were harvested in TRIzol Reagent (ThermoFisher) and RNA was isolated according to the manufacturer's instructions. DNA was removed with DNaseI treatment (NEB) and cDNA was prepared with M-MLV Reverse Transcriptase (Promega). The transcript levels were quantified using Power SYBR® Green PCR Master Mix (ThermoFisher) using the indicated primer (Appendix Table S5).

PAM2 motif alignment

Ortholog searches were performed using HaMStR-OneSeq (Ebersberger *et al*, 2013). Human MKRN1 and MKRN2 (UniProt identifiers: Q9UHC7, Q9H000) served as seed proteins and orthologs were searched within data from the Quest for Orthologs Consortium (release 2017_04; Sonnhammer *et al*, 2014). In order to identify functionally equivalent proteins, we calculated a unidirectional Feature Architecture Similarity (FAS) score that compares the domain architecture of the seed protein and the predicted ortholog (Koestler *et al*, 2010). Predicted orthologs with FAS < 0.7 were removed. The multiple sequence alignment of the PAM2 motifs of Makorin orthologs from selected arthropod and vertebrate species was generated using MAFFT v7.294b L-INS-i (Katoh and Standley, 2013). Since the PAM2 motif in all Makorin proteins differs from the described consensus, a PAM2 hidden Markov model was trained on Makorin PAM2 motifs and used for a HMMER scan (http://hmmer.org/) of the orthologs. Orthologs include species name, UniProt identifiers and amino acid (aa) positions of the PAM2 motif within the protein: *Drosophila melanogaster,* Q9VP20, 81-95 aa; *Anopheles gambiae,* Q7QF83, 57-71 aa; *Tribolium castaneum,*

A0A139WP96, 159-173 aa; *Ixodes scapularis,* B7QIJ9, 119-133 aa; human, Q9UHC7, 163-177 aa; mouse, Q9QXP6, 163-177 aa; zebrafish, Q4VBT5, 120-134 aa.

Acknowledgements

We would like to thank the Bloomington Drosophila Stock Center for fly reagents, and Anne Ephrussi, Craig Smibert, Daniel St Johnston, and Nahum Sonenberg for antibodies. We also thank Violeta Morin and Beili Hu for fly embryo injections, the IMB Proteomics Core Facility for the initial analysis of the mass spectrometry data and the IMB Core Facility Genomics for their helpful support. This work was supported by CIHR grants MOP-44050 and IOP-107945 to P.L., by the Deutsche Forschungsgemeinschaft (DFG) SPP1935 Grants RO 4681/4-1 to J.Y.R and KO 4566/3-1 to J.K.

Author Contributions

A.D., H.H. and N.L. performed the experiments and wrote the draft of the manuscript. A.H. performed MS experiments and iCLIP libraries. A.B. analyzed MS experiments. M.B. and A.B. analyzed iCLIP data. C.R. analyzed and identified the PAM2 motif. P.B., K.Z. and J.K. guided the MS and iCLIP experiments. J.Y.R. and P.L. supervised the project and finalized the manuscript.

Conflict of interest

The authors have no conflicts of interest to report.

References

Besse F, López de Quinto S, Marchand V, Trucco A, Ephrussi A. 2009. *Drosophila* PTB promotes formation of high-order RNP particles and represses *oskar* translation. *Genes Dev* **23**: 195-207.

Bohne A, Darras A, D'Cotta H, Baroiller JF, Galiana-Arnoux D, Volff, JN. 2010. The vertebrate makorin ubiquitin ligase gene family has been shaped by large-scale duplication and retroposition from an ancestral gonad-specific, maternal-effect gene. *BMC Genomics* **11**: 721.

Breitwieser W, Markussen FH, Horstmann H, Ephrussi A. 1996. Oskar protein interaction with Vasa represents an essential step in polar granule assembly. *Genes Dev* **10**: 2179-2188.

Carpenedo RL, Cassar PA, Stanford WL. 2016. MKRN1: Uncovering function by an unbiased systems approach. *Cell Cycle* **15**: 303-304.

Cassar PA, Carpenedo RL, Samavarchi-Tehrani P, Olsen JB, Park CJ, Chang WY, Chen Z, Choey C, Delaney S, Guo H, Guo H, Tanner RM, Perkins TJ, Tenenbaum SA, Emili A, Wrana JL, Gibbings D, Stanford WL. 2015. Integrative genomics positions MKRN1 as a novel ribonucleoprotein within the embryonic stem cell gene regulatory network. *EMBO Rep* **10**: 1334-1357.

Castagnetti S, Ephrussi A. 2003. Orb and a long poly(A) tail are required for efficient *oskar* translation at the posterior pole of the *Drosophila* oocyte. *Development* **130**: 835-843.

Chang CW, Nashchekin D, Wheatley L, Irion U, Dahlgaard K, Montague TG, Hall J, St Johnston D. 2011. Anterior-posterior axis specification in *Drosophila* oocytes: identification of novel *bicoid* and *oskar* mRNA localization factors. *Genetics* **188:** 883-896.

Chang JS, Tan L, Schedl P. 1999. The *Drosophila* CPEB homolog, *orb*, is required for Oskar protein expression in oocytes. *Dev Biol* **215**: 91-106.

Chekulaeva M, Hentze MW, Ephrussi A. 2006. Bruno acts as a dual repressor of *oskar* translation, promoting mRNA oligomerization and formation of silencing particles. *Cell* **124**: 521-533.

Chou TB, Perrimon N. 1996. The autosomal FLP-DFS technique for generating germline mosaics in *Drosophila melanogaster. Genetics* **144**: 1673-1679.

Clouse KN, Ferguson SB, Schüpbach T. 2008. Squid, Cup, and PABP55B function together to regulate *gurken* translation in *Drosophila*. *Dev Biol* **313**: 713-724.

Ebersberger I, Simm S, Leisegang MS, Schmitzberger P, Mirus O, von Haeseler A, Bohnsack MT, Schleiff E. 2014. The evolution of the ribosome biogenesis pathway from a yeast perspective. *Nucleic Acids Res* **42**: 1509-1523.

Ephrussi A, Dickinson LK, Lehmann R. 1991. Oskar organizes the germ plasm and directs localization of the posterior determinant nanos. *Cell* **66**: 37-50.

Ephrussi A, Lehmann, R. 1992. Induction of germ cell formation by *oskar*. *Nature* **358**: 387-392.

Filardo P, Ephrussi A. 2003. Bruno regulates *gurken* during *Drosophila* oogenesis. *Mech Dev* **120**: 289-297.

Geng C, Macdonald PM. 2006. Imp associates with Squid and Hrp48 and contributes to localized expression of Gurken in the oocyte. *Mol Cell Biol* **26**: 9508-9516.

Gray TA, Hernandez L, Carey AH, Schaldach MA, Smithwick, MJ, Rus K, Marshall Graves JA, Stewart CL, Nicholls RD. The ancient source of a distinct gene family encoding proteins featuring RING and C(3)H zinc-finger motifs with abundant expression in developing brain and nervous system. *Genomics* **66**: 76-86.

Herrera RA, Kiontke K, Fitch DH. 2016. Makorin ortholog LEP-2 regulates LIN-28 stability to promote the juvenile-to-adult transition in *Caenorhaebditis elegans. Development* **143**: 799-809.

Hrdlicka L, Gibson M, Kiger A, Micchelli C, Schober M, Schöck F, Perrimon N. 2002. Analysis of twenty-four Gal4 lines in *Drosophila melanogaster. Genesis* **34**: 51-57.

Huppertz I, Attig J, D'Ambrogio A, Easton LE, Sibley CR, Sugimoto Y, Tajnik M, König J, Ule J. 2014. iCLIP: protein-RNA interactions at nucleotide resolution. *Methods* **65**: 274-287.

Jambor H, Surendranath V, Kalinka AT, Mejstrik P, Saalfeld S, Tomancak P. 2015. Systematic imaging reveals features and changing localization of mRNAs in *Drosophila* development. *eLife* **4**. doi 10.7554/eLife.05003.

Katoh K, Standley DM. 2013. MAFFT multiple sequence alignment software version 7: improvements in performance and usability. *Mol Biol Evol* **30**: 772-780.

Kim G, Pai C-I, Sato K, Person MD, Nakamura A, Macdonald PM. 2015. Region-specific activation of *oskar* mRNA translation by inhibition of Bruno-mediated repression. *PLoS Genet* **11(2)**: e1004992.

Kim JH, Park SM, Kang MR, Oh SY, Lee TH, Muller MT, and Chung IK. 2005. Ubiquitin ligase MKRN1 modulates telomere length homeostasis through a proteolysis of hTERT. *Genes Dev* **19**: 776-781.

Kim-Ha J, Kerr K, Macdonald PM. 1995. Translational regulation of *oskar* mRNA by Bruno, an ovarian RNA-binding protein, is essential. *Cell* **81**: 403-412.

Koestler T, von Haeseler A, Ebersberger I. 2010. FACT: functional annotation transfer between proteins with similar feature architectures. *BMC Bioinformatics* **11**: 417.

Lasko PF, Ashburner M. 1990. Posterior localization of Vasa protein correlates with, but is not sufficient for, pole cell development. *Genes Dev* **4**: 905-921.

Lasko P. 2012. mRNA localization and translational control in *Drosophila* oogenesis. *Cold Spring Harb Perspec Biol* **4(10)**: a012294.

Lécuyer E, Yoshida H, Parthasarathy N, Alm C, Babak T, Cerovina T, Hughes TR, Tomancak P, Krause HM. 2007. Global analysis of mRNA localization reveals a prominent role in organizing cellular architecture and function. *Cell* **131**: 174-187.

Lécuyer E, Parthasarathy N, Krause HM. 2008. Fluorescent in situ hybridization protocols in *Drosophila* embryos and tissues. *Methods Mol Biol* **420**: 289-302.

Lehmann R, Nüsslein-Volhard C. 1986. Abdominal segmentation, pole cell formation, and embryonic polarity require the localized activity of *oskar*, a maternal gene in *Drosophila*. *Cell* **47**: 141-152.

Lehmann R. 2016. Germ plasm biogenesis--an Oskar-centric perspective. *Curr Top Dev Biol* **116**: 679-707.

Lence T, Akhtar J, Bayer M, Schmid K, Spindler L, Ho CH, Kreim N, Andrade-Navarro MA, Poeck B, Helm M, Roignant JY. 2016. m^6A modulates neuronal functions and sex determination in *Drosophila. Nature* **540**: 242-247.

Liu N, Lasko P. 2015. Analysis of RNA interference lines identifies new functions of maternally-expressed genes involved in embryonic patterning in *Drosophila melanogaster*. *G3 (Bethesda)* **5**: 1025-1034.

Mahowald AP. 2001. Assembly of the *Drosophila* germ plasm. *Int Rev Cytol* **203**: 187-213.

Manseau L, Calley J, Phan H. 1996. Profilin is required for posterior patterning of the *Drosophila* oocyte. *Development* **122**: 2109-2116.

Markussen F-H, Michon A-M, Breitwieser W, Ephrussi A. 1995. Translational control of *oskar* generates Short OSK, the isoform that induces pole plasm assembly. *Development* **121**: 3723-3732.

McDermott SM, Meignin C, Rappsilber J, Davis I. 2012. *Drosophila* Syncrip binds the *gurken* mRNA localisation signal and regulates localised transcripts during axis specification. *Biol Open* **1**: 488-497.

Micklem DR, Adams J, Grünert S, St Johnston D. 2000. Distinct roles of two conserved Staufen domains in *oskar* mRNA localization and translation. *EMBO J* **19**: 1366-1377.

Miroci H, Schob C, Kindler S, Olschlager-Schutt J, Fehr S, Jungenitz T, Schwarzacher SW, Bagni C, Mohr E. 2012. Makorin ring zinc finger protein 1 (MKRN1), a novel poly(A)-binding protein-interacting protein, stimulates translation in nerve cells. *J Biol Chem* **287**: 1322-1334.

Munro TP, Kwon S, Schnapp BJ, St Johnston D. 2006. A repeated IMP-binding motif controls *oskar* mRNA translation and anchoring independently of *Drosophila melanogaster* IMP. *J Cell Biol* **172**: 577-588

Na H, Laver JD, Jeon J, Singh F, Ancevicius K, Fan Y, Cao WX, Nie K, Yang Z, Luo H et al. 2016. A high-throughput pipeline for the production of synthetic antibodies for analysis of ribonucleoprotein complexes. *RNA* **22**: 636-655.

Nakamura A, Amikura R, Hanyu K, Kobayashi S. 2001. Me31B silences translation of oocyte-localizing RNAs through the formation of cytoplasmic RNP complex during *Drosophila* oogenesis. *Development* **128**: 3233-3242.

Nakamura A, Sato K, Hanyu-Nakamura K. 2004. *Drosophila* Cup is an eIF4E binding protein that associates with Bruno and regulates *oskar* mRNA translation in oogenesis. *Dev Cell* **6**: 69-78.

Norvell A, Debec A, Finch, D, Gibson L, Thoma B. 2005. Squid is required for efficient posterior localization of *oskar* mRNA during *Drosophila* oogenesis. *Dev Genes Evol* **215**: 340-349.

Nüsslein-Volhard C, Frohnhöfer HG, Lehmann R. 1987. Determination of anteroposterior polarity in *Drosophila. Science* **238**: 1675-1681.

Qian X, Wang L, Zheng B, Shi ZM, Ge X, Jiang CF, Qian YC, Li DM, Liu X, Yin Y, et al. 2016. Deficiency of Mkrn2 causes abnormal spermiogenesis and spermiation, and impairs male fertility. *Sci Rep* **6**: 39318.

Reveal B, Yan N, Snee MJ, Pai CI, Gim Y, Macdonald PM. 2010. BREs mediate both repression and activation of *oskar* mRNA translation and act in trans. *Dev Cell* **18**: 496-502.

Reveal B, Garcia C, Ellington A, Macdonald PM. 2011. Multiple RNA binding domains of Bruno confer recognition of diverse binding sites for translational repression. *RNA Biol* **8**: 1047-1060.

Rongo C, Gavis ER, Lehmann R. 1995. Localization of *oskar* RNA regulates *oskar* translation and requires Oskar protein. *Development* **121**: 2737-2746.

Ryu YH, Macdonald PM. 2015. RNA sequences required for the noncoding function of *oskar* RNA also mediate regulation of Oskar protein expression by Bicoid Stability Factor. *Dev Biol* 407: 211-223.

Schüpbach T, Wieschaus E. 1991. Female sterile mutations on the second chromosome of *Drosophila melanogaster. Genetics* **129**: 1119-1136.

Shapiro RS, Anderson KV. 2006. *Drosophila* Ik2, a member of the I kappa B kinase family, is required for mRNA localization during oogenesis. *Development* **133**: 1467-1475.

Smith JL, Wilson JE, Macdonald PM. 1992. Overexpression of *oskar* directs ectopic activation of *nanos* and presumptive pole cell formation in *Drosophila* embryos. *Cell* **70**: 849-859.

Sonnhammer EL, Gabaldón T, Sousa da Silva AW, Martin M, Robinson-Rechavi M, Boeckmann B, Thomas PD, Dessimoz C, Quest for Orthologs consortium. 2014. Big data and other challenges in the quest for orthologs. *Bioinformatics* **30**: 2993-2998.

Steinhauer J, Kalderon D. 2005. The RNA-binding protein Squid is required for the establishment of anteroposterior polarity in the *Drosophila* oocyte. *Development* **132**: 5515-5525.

Tomancak P, Berman BP, Beaton A, Weiszmann R, Kwan E, Hartenstein V, Celniker SE, Rubin GM. 2007. Global analysis of patterns of gene expression during *Drosophila* embryogenesis. *Genome Biol.* **8**: R145.

Vazquez-Pianzola P, Urlaub H, Suter B. 2011. pAbp binds to the *osk* 3'UTR and specifically contributes to *osk* mRNA stability and oocyte accumulation. *Dev Biol* **357**: 404-418.

Wang C, Lehmann R. 1991. Nanos is the localized posterior determinant in *Drosophila*. *Cell* **66**: 637-647.

Webster PJ, Liang L, Berg CA, Lasko P, Macdonald PM. 1997. Translational repressor Bruno plays multiple roles in development and is widely conserved. *Genes Dev* **11**: 2510-2521.

Wilhelm JE, Hilton M, Amos Q, Henzel WJ. 2003. Cup is an eIF4E binding protein required for both the translational repression of *oskar* and the recruitment of Barentsz. *J Cell Biol* **163**: 1197-1204.

Wilson JE, Connell JE, Macdonald PM. 1996. *aubergine* enhances *oskar* translation in the *Drosophila* ovary. *Development* **122**: 1631-1639.

Zimyanin VL, Belaya K, Pecreaux J, Gilchrist MJ, Clark A, Davis I, St Johnston D. 2008. In vivo imaging of *oskar* mRNA transport reveals the mechanism of posterior localization. *Cell* **134**: 843-853.

Figure Legends

Figure 1. *Mkrn1* alteration affects ovarian development.

A. Relative *Mkrn1* mRNA levels at various stages of development, as measured by quantitative RT-PCR. Error bars depict Stdev, n=3 (technical replicates only).

B. Schematic diagram of the proteins encoded by the *Mkrn1* alleles used to analyze its function in vivo. $Mkrn1^{N}$ is a null allele and produces no protein.

C-F Bright-field micrographs of entire ovaries from wild-type and *Mkrn1* mutants. Note the reduced size of $Mkrn1^{S}$ and $Mkrn1^{N}$ ovaries.

G-J Individual egg chambers stained with the DNA stain DAPI. Fewer stage-10 and older egg chambers are present in $Mkrn1^{S}$ and no late stage egg chambers are present in $Mkrn1^{N}$ ovaries. Abscission defects resulting from inappropriate follicle cell migration are frequently observed in $Mkrn1^{N}$ ovaries (J, arrow).

K-N Individual egg chambers stained with α-Lamin to highlight nuclear membranes. (M) The oocyte nucleus (marked with an arrow in K, L, and M) remains at the posterior of $Mkrn1^{S}$ oocytes. (N) Some $Mkrn1^{N}$ egg chambers have 16 germline cells whose

nuclei are all of similar size, suggesting a defect in oocyte differentiation. Note also irregularities in the follicle cell monolayer in the *Mkrn1*^{N} egg chamber.

O-Q Dark field photographs of eggs and embryos produced by wild-type and *Mkrn1* mutants. (P) Most embryos produced by *Mkrn1*^{W} females have a posterior-group phenotype. (Q) Eggs produced by *Mkrn1*^{S} females lack dorsal appendages and do not support embryonic development. Scale bars, 20 μm.

Figure 2. Mkrn1 accumulates in pole plasm.

A-C The three panels show the same egg chambers stained for (A) Venus-Mkrn1, (B) Stau, and a (C) merged image. Colocalization of Venus-Mkrn1 and Stau can be observed in particles that have not yet accumulated at the posterior of the early stage 8 oocyte.

D-F The three panels show the same stage 10 egg chamber stained for (D) Venus-Mkrn1, (E) Stau and (F) a merged image. There is extensive colocalization of Venus-Mkrn1 and Stau in the posterior pole plasm of the oocyte.

G-I The three panels show the same egg chambers stained for (G) Venus-Mkrn1, (H) *osk* mRNA, and (I) a merged image. Colocalization of Venus-Mkrn1 and *osk* can be observed in an early stage 8 oocyte where *osk* has not yet fully localized at the posterior of the oocyte.

J-L The three panels show the same stage 10 egg chamber stained for (J) Venus-Mkrn1, (K) *osk* mRNA and (L) a merged image. There is extensive colocalization of Venus-Mkrn1 and *osk* mRNA in the posterior pole plasm of the oocyte.

M, N Venus-Mkrn1 expressed in an *osk*^{54}*/Df(3R)p-XT103* genetic background. Venus-Mkrn1 fails to accumulate in pole plasm.

O, P Venus-Mkrn1 expressed in a *vas*^{1}*/vas*^{PH} genetic background. Venus-Mkrn1 accumulates normally in pole plasm. Scale bars, 25 μm.

Figure 3. Mkrn1 mutations affect accumulation of proteins involved in axis patterning.

A-D Posterior accumulation of Osk is greatly reduced in stage 10 *Mkrn1*^{W} and *Mkrn1*^{S} oocytes as compared with wild-type. Osk is nearly undetectable in *Mkrn1*^{N} egg chambers. Scale bars, 25 μm.

E-H Posterior accumulation of Stau is greatly reduced in stage 10 *Mkrn1*^{W} and *Mkrn1*^{S} oocytes as compared with wild-type. Stau is nearly undetectable in *Mkrn1*^{N} egg chambers. Scale bars, 25 μm.

I-L Anterodorsal accumulation of Grk is normal in stage 10 *Mkrn1*^{W} oocytes. Grk remains associated with the oocyte nucleus and is mislocalized to the posterior in stage 10 *Mkrn1*^{S} oocytes. Grk is present at uniformly low levels or undetectable levels in all germ cells in *Mkrn1*^{N} egg chambers. Scale bars, (I-K) 20 μm, (L) 25 μm.

M-P Posterior accumulation of Aub is greatly reduced in stage 10 *Mkrn1*^{W} and *Mkrn1*^{S} oocytes as compared with wild-type. Aub is present at uniform levels in all germ cells in *Mkrn1*^{N} egg chambers. Scale bars, 20 μm.

Q-T Posterior accumulation of Vas is greatly reduced in stage 10 *Mkrn1*^{W} and *Mkrn1*^{S} oocytes as compared with wild-type. Vas is present at uniform levels in all germ cells in *Mkrn1*^{N} egg chambers. Scale bars, 25 μm.

U-X Accumulation of Orb is similar in wild-type and *Mkrn1*^{W} oocytes, but Orb is more concentrated in the posterior of *Mkrn1*^{S} oocytes. In early-stage *Mkrn1*^{N} egg chambers there is usually a single Orb-positive cell, indicating that some steps toward oocyte differentiation are able to take place. Scale bars, (U-W) 20 μm, (X) 25 μm.

Figure 4. *grk* and *osk* mRNAs are mislocalized in *Mkrn1* mutants.

A, B Anterodorsal accumulation of *grk* is similar to wild-type in stage 10 $Mkrn1^{W}$ oocytes.

C. *grk mRNA* remains associated with the oocyte nucleus and is mislocalized to the posterior in stage 10 $Mkrn1^{S}$ oocytes.

D, E As compared with (D) wild-type *osk* mRNA tends to accumulate in a focus slightly anterior to the posterior pole in (E) stage 10 $Mkrn1^{W}$ oocytes.

F. *osk* mRNA is essentially uniformly distributed in $Mkrn1^{S}$ oocytes.

G. Western blot analysis from ovary lysates of various genotypes stained for Osk, pAbp and β-Tubulin. Osk protein levels are greatly reduced in all *Mkrn1* mutant alleles.

H. RT-qPCR experiments measuring ovarian mRNA levels of *osk* and *grk* mRNA in the same genotypes as (G). Error bars depict Stdev, n=3 (technical replicates only).

Data information: (A-F) Scale bars, 50 μm.

Figure 5. Mkrn1 interacts strongly with poly(A) binding protein.

A. Western blot analysis of co-IP experiments between Venus-Mkrn1 and pAbp. a-Tubulin (lanes 1, 2) and ovaries lacking the Venus-Mkrn1 transgene (lane 4) were used as negative controls.

B. Summary of co-IP experiments between Myc- or GFP-tagged interacting proteins and $Mkrn1^{RING}$. The relative enrichment of $Mkrn1^{RING}$ signal in each IP compared to controls are depicted for three individual experiments.

C. Co-expression of pAbp stabilizes Mkrn1. FLAG-Mkrn1 was co-transfected with increasing levels of HA-pAbp in S2R+ cells. Left: Proteins were examined using immunoblotting. Right: Intensities of FLAG-Mkrn1 levels were quantified and normalized to intensities of β-tubulin. The relative intensity was normalized to *Mkrn1* mRNA levels analyzed by qPCR.

D. PAM2 motif alignment in different species. Comparison between *Drosophila* and human PAM2 motif revealed a Glu to Val substitution (blue) in the consensus sequence. The conserved amino acid sequence to *Drosophila* (dark purple) is indicated below. The PAM2 motif was mutated using two amino acid substitutions at positions 90 and 92 to alanine (F90A and P92A).

E. Western blot analysis of co-IP experiments of FLAG-Mkrn1 and pAbp. The interaction of pAbp and Mkrn1 is reduced when the PAM2 motif is mutated.

Figure 6. Mkrn1 associates specifically with the 3'UTR of *osk* mRNA.

A. RIP experiment showing that FLAG-Mkrn1 associates with *osk* mRNA, but not with *grk* or *bcd* mRNA. Either FLAG-tagged Mkrn1 or Mkrn1$^{\Delta ZnF1}$ was overexpressed in *Mkrn1*^{N} ovaries using the *nos>GAL4* driver. Enrichment of different transcripts was analyzed by RT-qPCR using primers that bind to the respective 3'UTRs. n=3.

B. iCLIP results showing specific binding of Mkrn1 to *osk* in a region of the 3'UTR that partially overlaps with the BRE-C (yellow). The crosslinking events indicate the interaction site of Mkrn1 to *osk* 3'UTR (purple). The Mkrn1 binding site is upstream of an A-rich sequence (AR, green). Data of six technical replicates for FLAG-Mkrn1 are combined.

C-E RIP experiments of FLAG-Mkrn1^{RING} in S2R+ cells. Enrichment of *luciferase-osk*-3'UTR transcript was analyzed by RT-qPCR. Relative change in binding compared to *luciferase-osk*-3'UTR or control knock down is depicted. n ≥ 3. (C) RIP experiment showing that Mkrn1^{RING} binding to *osk* 3'UTR is compromised by a deletion of the Mkrn1 binding site (*osk*$^{\Delta Mkrn1}$). (D) Binding of Mkrn1^{RING} to *osk* 3'UTR is reduced when using a deletion of the A-rich region of *osk* 3'UTR (*osk*$^{\Delta AR}$) (Vazquez-Pianzola et al., 2011). (E) RIP experiments were performed in either control cells or upon depletion of Imp or pAbp. Depletion of pAbp compromises binding of Mkrn1.

F. RIP experiments showing that FLAG-Mkrn1 binding to *luciferase-osk*-3'UTR is dependent on the ZnF1 domain as well as on the PAM2 motif. Enrichment was analyzed using RT-qPCR and relative change in binding compared to RIP of FLAG-Mkrn1 is illustrated. $n \geq 3$.

Data information: In (A, C-F) data are presented as mean; SEM. n.s. $P > 0.5$, ***$P \leq 0.001$, ****$P \leq 0.0001$ (paired t-test).

Figure 7. Mkrn1 competes with Bru for binding to *osk* mRNA.

A. RIP experiments examining the binding of different proteins to *luciferase-osk*-3'UTR performed in either control cells, or upon knockdown of Mkrn1. Binding of the indicated proteins to *luciferase-osk*-3'UTR was monitored by RT-qPCR. The relative fold change in recovered RNA upon Mkrn1 knockdown is illustrated. n=4.

B. Bru binding to *luciferase-osk*-3'UTR upon *pAbp* knockdown was analyzed using RT-qPCR. The relative fold change in binding of GFP-Bru to *luciferase-osk*-3'UTR compared to control knockdown is shown. n=3.

C. RIP experiments in either control (ctrl) or $Mkrn1^{W}$ ovaries using α-Bru antibody. The relative fold change in recovered endogenous *osk* RNA compared to $Mkrn1^{W}$ ovaries is shown. n=3.

D-G Immunostaining experiments showing Bru distribution in (D-E) wild-type and (F-G) $Mkrn1^{W}$ early-stage egg chambers. Note the more prominent accumulation of Bru in the oocyte in the *Mkrn1* mutant. Scale bars, (D, F) 25 μm; (E, G) 20 μm.

H-M Stage-10 egg chambers of the genotypes indicated immunostained with α-Osk. Posterior accumulation of Osk is restored to a variable degree (K-M) in $Mkrn1^{W}$ oocytes when heterozygous for *bru1*. Scale bars, 25 μm.

N. Model depicting activation of *osk* translation via Mkrn1. Mkrn1 and pAbp are recruited to the *osk* 3' UTR, displacing Bru and promoting translation initiation at the posterior pole.

Data information: In (A-C) data are presented as mean; error bars depict SEM. n.s. $P > 0.5$, $^{**}P \leq 0.01$, $^{****}P \leq 0.0001$ (paired t-test).

Expanded View Figure Legends

Figure EV1. Four *Makorin*-related genes in *Drosophila melanogaster*.

A. Sequence alignment of human MKRN1 and Mkrn1, CG5334, CG5347, and CG12477, the four Makorin-related proteins in *Drosophila melanogaster*. The ZnF1 domain in Mkrn1 is highlighted green, the PAM2 motif is highlighted yellow, the RING domain is highlighted red, and the ZnF2 domain is highlighted light blue. The RING and ZnF2 domains are conserved in all four proteins, whereas the PAM2 domain is only conserved in CG12477 and CG5347, and ZnF1 is conserved in CG5334 and CG5347.

B. Relative mRNA levels of *Mkrn1* and the three other genes encoding predicted Makorin proteins at various stages of development, as measured by RT-qPCR. Levels of *Mkrn1* were normalized to *rpl15* mRNA. Error bars depict Stdev, n=3 (technical replicates only).

Figure EV2. Further analysis of *Mkrn1* phenotypes.

A. Immunostaining with α-Vas reveals the absence of pole cells in $Mkrn1^{W}$ embryos.

B. DAPI staining of ovaries from females with genotypes indicated. Deletion of *Mkrn1* in germline cells only produces a phenotype similar to that of $Mkrn1^{N}$.

C. Vas immunostaining staining of ovaries from wild-type and from female expressing shRNA targeting *Mkrn1* under the control of the T155 driver that is active in follicle cells (T155>*Mkrn1* RNAi). No deleterious phenotype is observed in the latter.

Figure EV3. Further evidence for extensive co-localization of Venus-Mkrn1 with pole plasm components.

All images are from wild-type oocytes expressing Venus-Mkrn1 or FLAG-Mkrn1 as indicated. (A, D, M, P, S, V) Immunostaining with α-GFP recognizing Venus-Mkrn1. (G, J) Immunostaining with a-FLAG recognizing FLAG-Mkrn1. (B, E) Immunostaining with α-Stau. (H, K) Immunostaining with α-Osk. (N, Q) Immunostaining with α-Vas. (T, W) Immunostaining with α-Aub. (C, F, I, L, O, R, U, X) Merged images from two preceding panels.

Figure EV4. Effects of *osk* and *vas* mutations on Mkrn1 localization.

A. Posterior accumulation of either Venus-Mkrn1 or FLAG-Mkrn1 is normal in osk^{54}/*TM3,Sb* (*osk*/+) oocytes but is absent in osk^{54}/*Df(3R)p-XT103* (*osk*) oocytes.

B. Posterior accumulation of either Venus-Mkrn1 or FLAG-Mkrn1 is normal in both vas^{1}/+ (*vas*/+) *or* vas^{1}/vas^{PH} (*vas*) oocytes.

Figure EV5. Mkrn1 genetically interacts with *osk* and *vas*.

A. Pole cell counts from embryos produced by females with the genotypes listed. Embryos from trans-heterozygotes for *Mkrn1* and *osk* or *vas* mutations have fewer pole cells than those from single heterozygote controls. Depicted is Stdev, n=60.

B-J Multiple images of *Mkrn1* mutant egg chambers showing variability of effects on Stau and Grk localization. (B-D) $Mkrn1^{W}$ egg chambers immunostained with α-Stau. (E-G) Multiple images of $Mkrn1^{W}$ egg chambers immunostained with α-Grk. (H-J) Multiple images of $Mkrn1^{S}$ egg chambers immunostained with α-Grk.

Figure EV6. Transgenic expression of tagged Mkrn1 rescues all *Mkrn1* mutant phenotypes.

A-C Bright-field micrographs of entire ovaries from (A) $Mkrn1^{N}$; (B) *nos>FLAG-Mkrn1*; $Mkrn1^{N}$ (C) wild-type females, showing overall rescue of oogenesis.

D-F α-Osk immunostaining on (D) $Mkrn1^{W}$, (E) $Mkrn1^{S}$, (F) $Mkrn1^{N}$ egg chambers as negative controls.

G-J Transgenic expression of tagged *Mkrn1* restores posterior localization of Osk protein in $Mkrn1^{W}$ oocytes. (G, H) *nos>Venus-Mkrn1;* $Mkrn1^{W}$*;* (I, J) *nos>FLAG-Mkrn1;* $Mkrn1^{W}$. (H, J) Immunostaining with α-Osk; (G) Immunostaining with α-GFP recognizing Venus-Mkrn1; (I) Immunostaining with α-FLAG recognizing FLAG-Mkrn1.

K-N Transgenic expression of tagged *Mkrn1* restores expression and posterior localization of Osk protein in $Mkrn1^{S}$ oocytes. (K, L) *nos>Venus-Mkrn1*; $Mkrn1^{S}$*;* (M, N) *nos>FLAG-Mkrn1*; $Mkrn1^{S}$. (L, N) Immunostaining with α-Osk; (K) Immunostaining with α-GFP recognizing Venus-Mkrn1; (M) Immunostaining with α-FLAG recognizing FLAG-Mkrn1.

O, P Transgenic expression of tagged *Mkrn1* restores expression and posterior localization of Osk protein in $Mkrn1^{N}$ oocytes.

Q-TImmunostaining experiments revealing localization of various proteins in *nos>Venus-Mkrn1;* $Mkrn1^{N}$ oocytes. (Q) α-Stau; (R) α-Vas; (S) α-Aub; (T) α-Grk.

Figure EV7. *Mkrn1* mutations affect accumulation of mRNAs involved in axis patterning in embryos.

In situ hybridization experiments showing posterior accumulation of (A, B) *osk*, (C, D) *nos*, and (E, F) *pgc* mRNAs in (A, C, E) wild-type embryos. (B, D, F) Posterior accumulation of these mRNAs is lost in some $Mkrn1^{W}$ embryos.

Figure EV8. Interactome of Mkrn1 in S2R+ cells.

A. Schematic diagram of Mkrn1 constructs with functional domains highlighted. $Mkrn1^{RING}$ carries a point mutation that changes histidine 239 to glutamic acid (H239E) while $Mkrn1^{\Delta ZnF1}$ contains a deletion of amino acids 26 to 33. To disrupt the ZnF2 domain ($Mkrn1^{ZnF2}$) three point mutations that change the cysteines to alanines at positions 302, 312 and 318 (C302A, C312A and C318A) were introduced.

B. Immunoblot showing the relative expression levels of various forms of FLAG-Mkrn1 in S2R+ cells.

C, D Volcano plot showing the interactome of (C) Myc-$Mkrn1^{RING}$ and (D) Myc-Mkrn1 in S2R+ cells as identified using mass spectrometry and label-free quantification. The enrichment of proteins compared to control was plotted in a volcano plot using a combined cutoff of $\log_2$ fold change of 2 and an FDR of 0.05. Several proteins of interest are labelled. The entire list of enriched proteins can be found in Appendix Tables S1 and S2.

Figure EV9. Validation of Mkrn1 interactome.

Pulldown experiments to validate associations of tagged $Mkrn1^{RING}$ with (A) GFP-pAbp, (B) GFP-Imp, (C) Myc-eIF4G (D) Myc-Sqd and (E) Myc-Me31B. GFP and Myc immunoprecipitation was performed in the absence or presence of RNase T1 and

enrichment of the proteins was analyzed by immunoblotting. (F) Western blot analysis of co-IP experiments between Venus-Mkrn1 and eIF4G. α-Tubulin (αtub, lanes 1, 2) and ovaries lacking the *Venus-Mkrn1* transgene (lane 4) were used as negative controls.

Figure EV10. Analysis of interaction strength between Mkrn1^{RING} and binding partners.

Representative western blots of co-IP experiments between Mkrn1^{RING} and (A) Myc-pAbp, (B) Myc-eIF4G, (C) Myc-me31B, (D) Myc-Sqd and (E) GFP-Imp using either 150 mM, 300 mM or 500 mM salt concentration for washing. The intensity of the Mkrn1^{RING} signal after IP was quantified and normalized to input levels. The resulting enrichment over control IP is summarized in Fig 5B.

Figure EV11. Analysis of the RNA binding ability of Mkrn1.

A. The RNA binding activity of Mkrn1 is mediated by its ZnF1 domain. Autoradiographs showing RNA binding to various forms of Mkrn1 and a GFP negative control. Crosslinked RNA-protein complexes were immunoprecipitated with α-FLAG and treated with different dilutions of RNase I (left: 1/50, right: 1/5000). RNA was subsequently radiolabelled and the RNA-protein complexes were separated by SDS-PAGE. Bound RNA of different sizes is detected by a smear extending upward from the sharp bands that correspond to the sizes of the FLAG-Mkrn1 proteins (arrow).

B. Representative immunoblot of RIP experiments shown in Fig 6A. Either Mkrn1 or Mkrn1$^{\Delta ZnF1}$ were overexpressed in *Mkrn1^{N}* ovaries using *nos>Gal4* driver. The proteins were pulled down using α-FLAG antibody.

C. Validation of iCLIP experiments. Immunoprecipitation of FLAG-Mkrn1 was performed in different conditions. S2R+ cells were transfected and UV-crosslinked prior to IP experiments. Left: autoradiograph showing protein-RNA complexes. Right:

Signals of lanes 2, 4 and 5 in autoradiograph were cut and RNA isolated. RNA length was analyzed on a TBE-urea gel.

Figure EV12. Mkrn1 binding to *osk* 3'UTR is dependent on pAbp.

A. Mkrn1^{RING} but not Mkrn1$^{\Delta ZnF1}$ binds to the *osk* 3' UTR in S2R+ cells. FLAG-RIP of GFP, Mkrn1^{RING} and Mkrn1$^{\Delta ZnF1}$ were performed in S2R+ cells co-expressing *luciferase-grk*-3'UTR and *luciferase-osk*-3'UTR reporter. Error bars depict Stdev, n=3 (technical replicates only).

B-E Western blot analysis of a representative RIP experiment summarized in Figs 6C-E. RIP of GFP or Mkrn1^{RING} were performed either in presence of *luciferase-osk*-3'UTR with wild-type sequence, (B) a mutation in the Mkrn1 binding site (*osk*$^{\Delta Mkrn1}$) or (C) a mutation in the AR region (*osk*$^{\Delta AR}$). RIP experiments against FLAG-Mkrn1^{RING} were performed in control (*LacZ*) condition and compared to (D) *Imp* or (E) *pAbp* mRNA knockdown. Right: RT-qPCR analysis of the knockdown efficiency. *Imp* and *pAbp* mRNA levels were normalized to *rpl15* mRNA.

F. FLAG-RIP experiments in S2R+ cells using different *Mkrn1* mutants. Representative immunoblot is depicted.

Figure EV13. Binding of Bru to *osk* 3'UTR is antagonized by Mkrn1.

A. RIP experiment of GFP alone (ctrl) or GFP-tagged Bru in S2R+ cells. Left: qPCR analysis of RIP experiment analyzing co-transfected *luciferase-osk*-3'UTR and endogenous *grk* mRNA. Error bars depict Stdev, n=3 (one experiment only). Right: Immunoblot of the IP .

B-D Immunoblots of representative RIP experiments summarized in Figs 7A-C. Right: RT-qPCR validation of the respective knockdown. mRNA levels were normalized to *rpl15* mRNA. (B) RIP experiment of either GFP alone, GFP-Imp or GFP-

Bru was performed in control (*LacZ*) or *Mkrn1* mRNA knockdown condition. (C) RIP experiment performed against FLAG-tagged pAbp or Sqd in knockdown condition of *LacZ* or *Mkrn1* mRNA. (D) GFP-RIP against either GFP alone or GFP-Bru in control or *pAbp* KD.

E. Representative immunoblot of a RIP experiment using control or $Mkrn1^{W}$ ovary lysate against endogenous Bru. As control IP, rabbit IgG was used.

F-Q Bru and *osk* mRNA co-localize in wild-type and $Mkrn1^{W}$ ovaries. (F, H, J) The three panels show the same wild-type stage 10 egg chamber stained for (E) Bru, (H) *osk* mRNA and (J) a merged image. There is faint accumulation of Bru in the pole plasm and therefore modest co-localization with *osk* mRNA. (G, I, K) Higher magnification images of the same wild-type stage 10 egg chamber stained for (G) Bru, (I) *osk* mRNA and (K) a merged image, but different from the egg chamber in (F, H, J), illustrating the same point. (L, N, P) The three panels show the same $Mkrn1^{W}$ stage 10 egg chamber stained for (L) Bru, (N) *osk* mRNA and (P) a merged image. There is accumulation of Bru near the pole plasm and co-localization with *osk* mRNA. (M, O, Q) Higher magnification images of the same $Mkrn1^{W}$ stage 10 egg chamber stained for (M) Bru, (O) *osk* mRNA and (Q) a merged image, illustrating the same point. (R-T) The three panels show the same $Mkrn1^{W}$ stage 10 egg chamber stained for (R) Stau, (S) *osk* mRNA and (T) a merged image. There is accumulation of Stau near the pole plasm and co-localization with *osk* mRNA.

Figure EV14. Mkrn1 does not influence binding nor ubiquitination of Bruno.

A, B Co-IP experiment of GFP-tagged Bru in S2R+ cells with (A) HA-Bru or (B) HA-Cup. GFP IP was performed in either control (*LacZ*) or *Mkrn1* mRNA KD condition. Left: Immunoblot. Right: qPCR was performed to analyze KD efficiency. mRNA levels of *Mkrn1* were normalized to *rpl15* mRNA.

C. Ubiquitination assay in S2R+ cells was performed in either *LacZ* or *Mkrn1* mRNA KD condition. Left: Ubiquitination of input and IP samples was analyzed via immunoblotting endogenous ubiquitin. Two different blots were prepared with 50% of IP each and stained either with α-GFP or α-ubiquitin. Right: qPCR analysis of the KD efficiency. mRNA levels of *Mkrn1* were normalized to *rpl15* mRNA.

Expanded View Table Legends

Table EV1.

Expression of tagged *Mkrn1* from transgenes rescues oogenesis and viability to embryos produced by *Mkrn1* mutant females.

Dold_Fig1

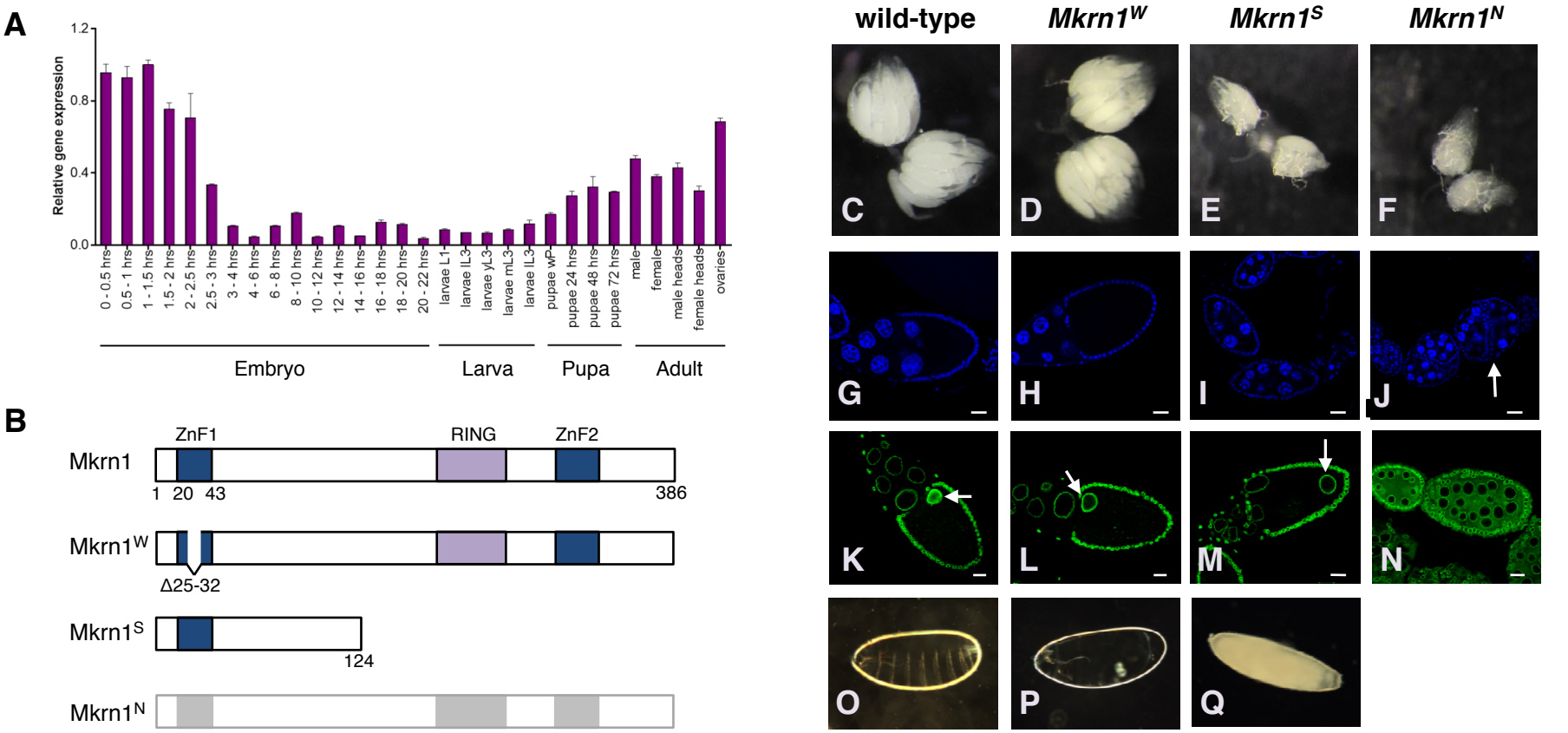
A
Relative gene expression
1.2
0.8
0.4
0.0
0 - 0.5 hrs
0.5 - 1 hrs
1 - 1.5 hrs
1.5 - 2 hrs
2 - 2.5 hrs
2.5 - 3 hrs
3 - 4 hrs
4 - 6 hrs
6 - 8 hrs
8 - 10 hrs
10 - 12 hrs
12 - 14 hrs
14 - 16 hrs
16 - 18 hrs
18 - 20 hrs
20 - 22 hrs
larvae L1
larvae lL3
larvae yL3
larvae mL3
larvae lL3
pupae wP
pupae 24 hrs
pupae 48 hrs
pupae 72 hrs
male
female
male heads
female heads
ovaries
Embryo
Larva
Pupa
Adult
B
ZnF1
RING
ZnF2
Mkrn1
1 20 43
386
Mkrn1W
Δ25-32
Mkrn1S
124
Mkrn1N
wild-type
Mkrn1W
Mkrn1S
Mkrn1N
C
D
E
F
G
H
I
J
K
L
M
N
O
P
Q

Dold_Fig2

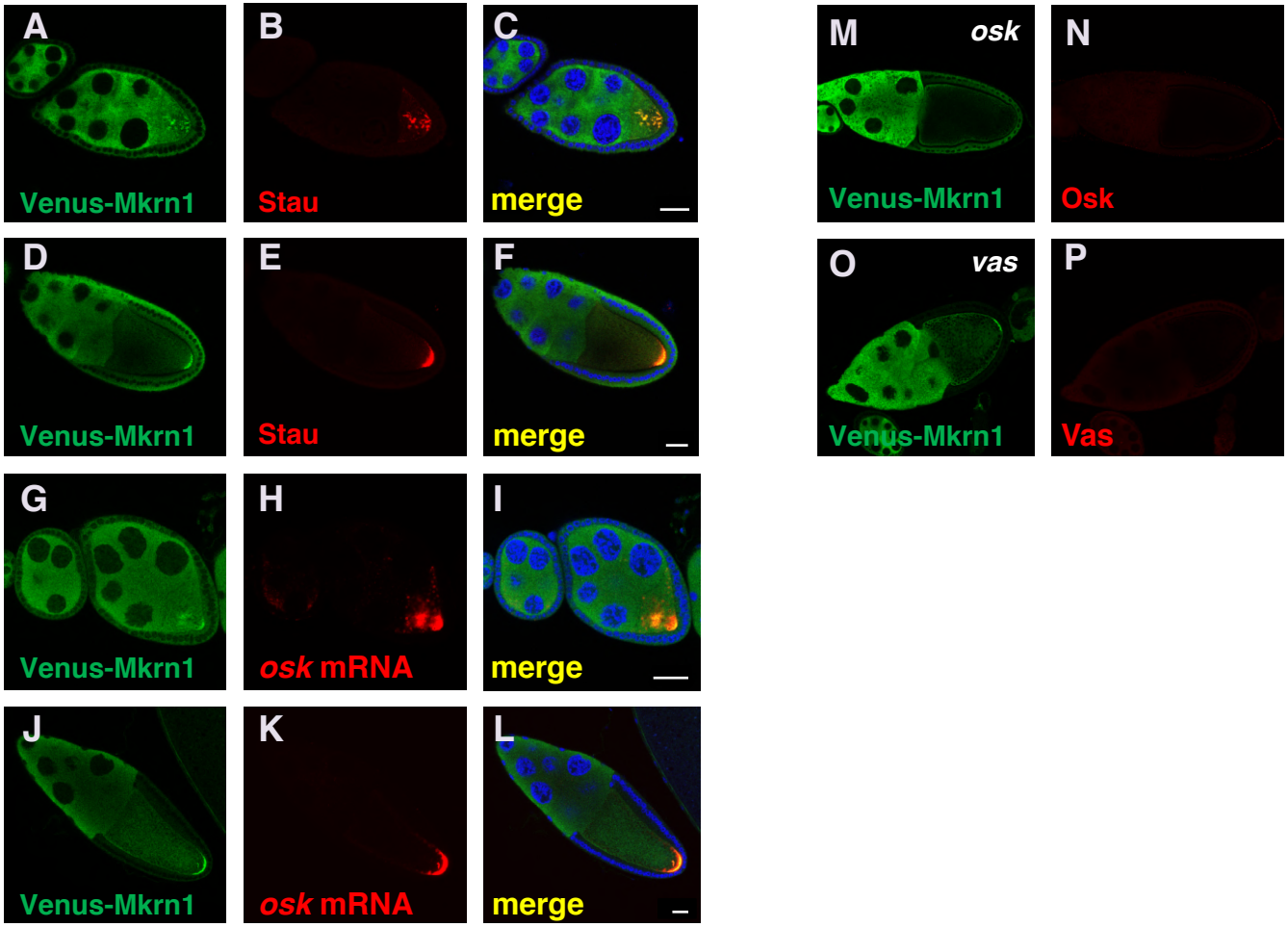
A
Venus-Mkrn1
B
Stau
C
merge
D
Venus-Mkrn1
E
Stau
F
merge
G
Venus-Mkrn1
H
osk mRNA
I
merge
J
Venus-Mkrn1
K
osk mRNA
L
merge
M
osk
Venus-Mkrn1
N
Osk
O
vas
Venus-Mkrn1
P
Vas

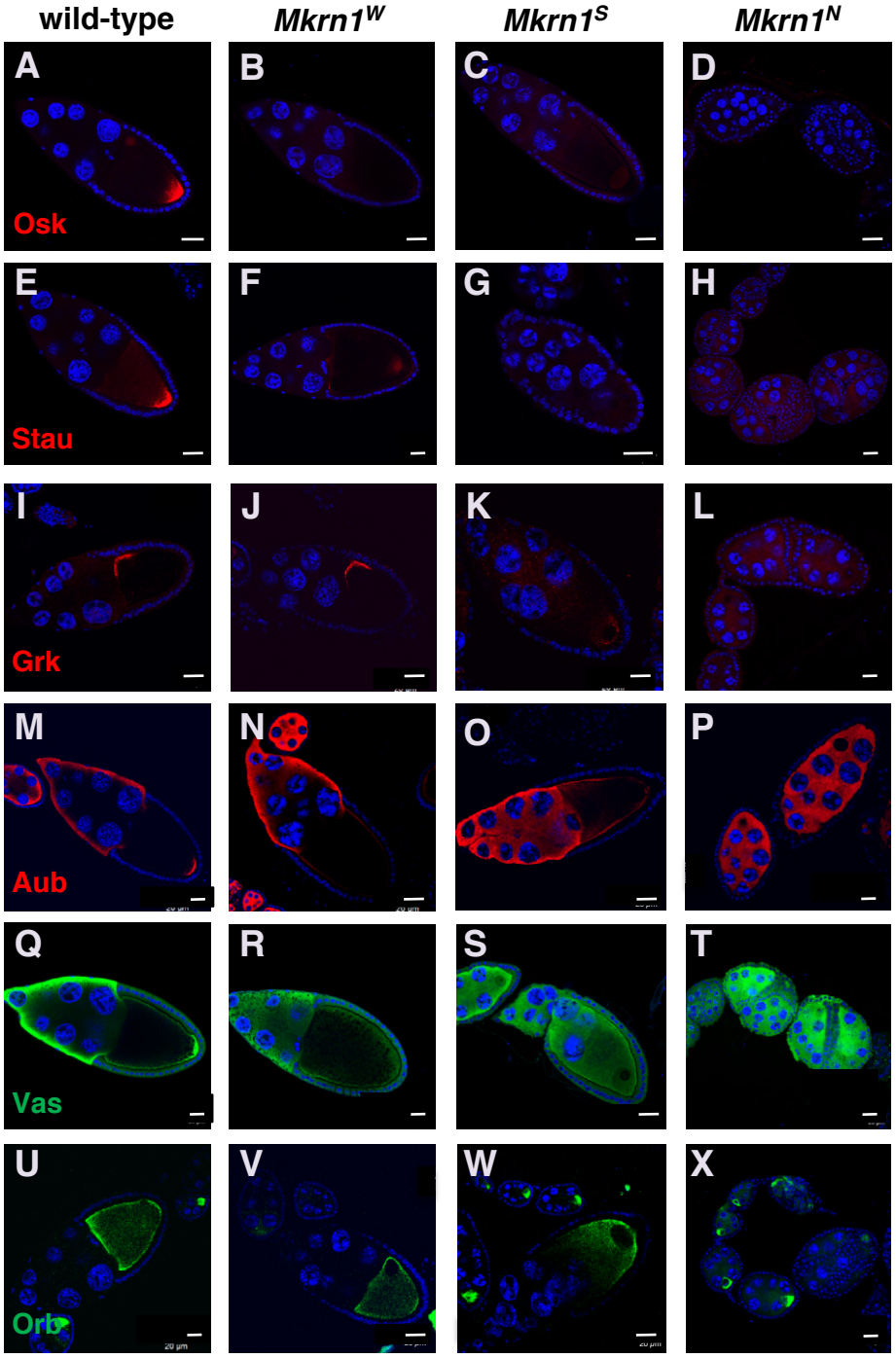
wild-type
Mkrn1W
Mkrn1S
Mkrn1N
A
B
C
D
Osk
E
F
G
H
Stau
I
J
K
L
Grk
M
N
O
P
Aub
Q
R
S
T
Vas
U
V
W
X
Orb

Dold_Fig3

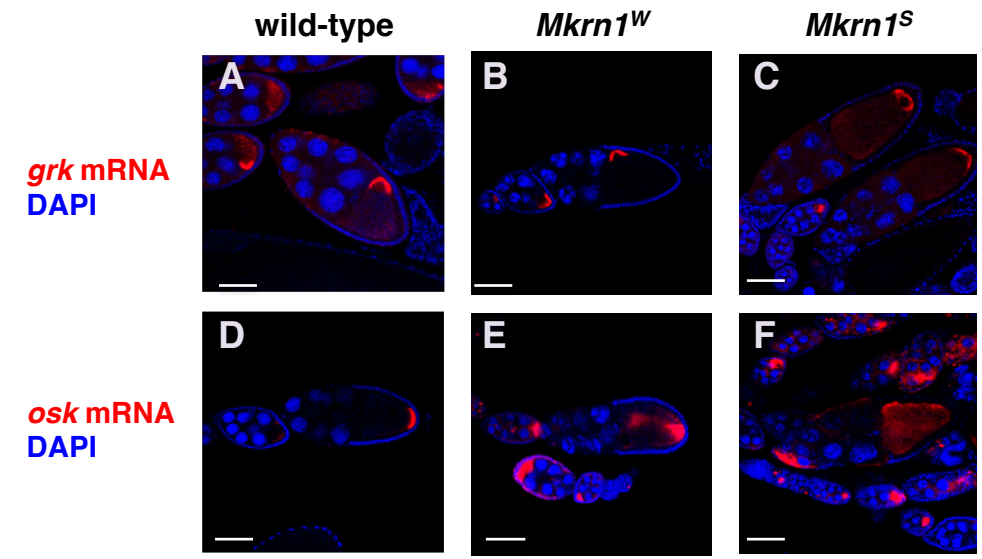
wild-type
Mkrn1W
Mkrn1S
grk mRNA
DAPI
osk mRNA
DAPI
A
B
C
D
E
F

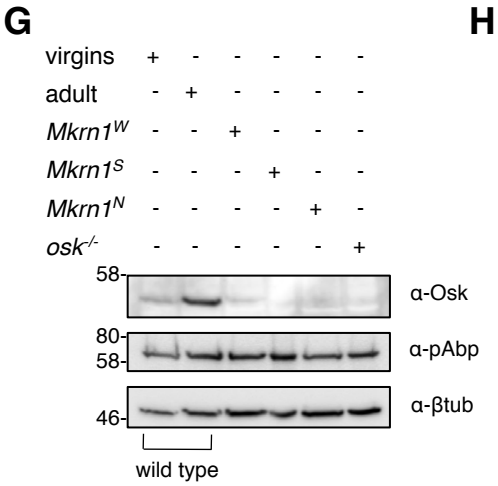
G
virgins + - - - - -
adult - + - - - -
Mkrn1W - - + - - -
Mkrn1S - - - + - -
Mkrn1N - - - - + -
osk-/- - - - - - +
58
α-Osk
80
58
α-pAbp
46
α-βtub
wild type

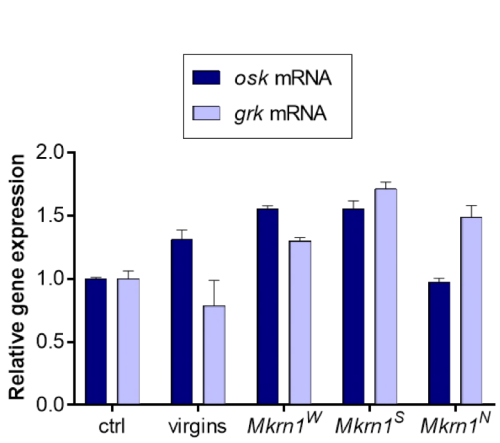
H
osk mRNA
grk mRNA
Relative gene expression
2.0
1.5
1.0
0.5
0.0
ctrl
virgins
Mkrn1W
Mkrn1S
Mkrn1N

Dold_Fig5

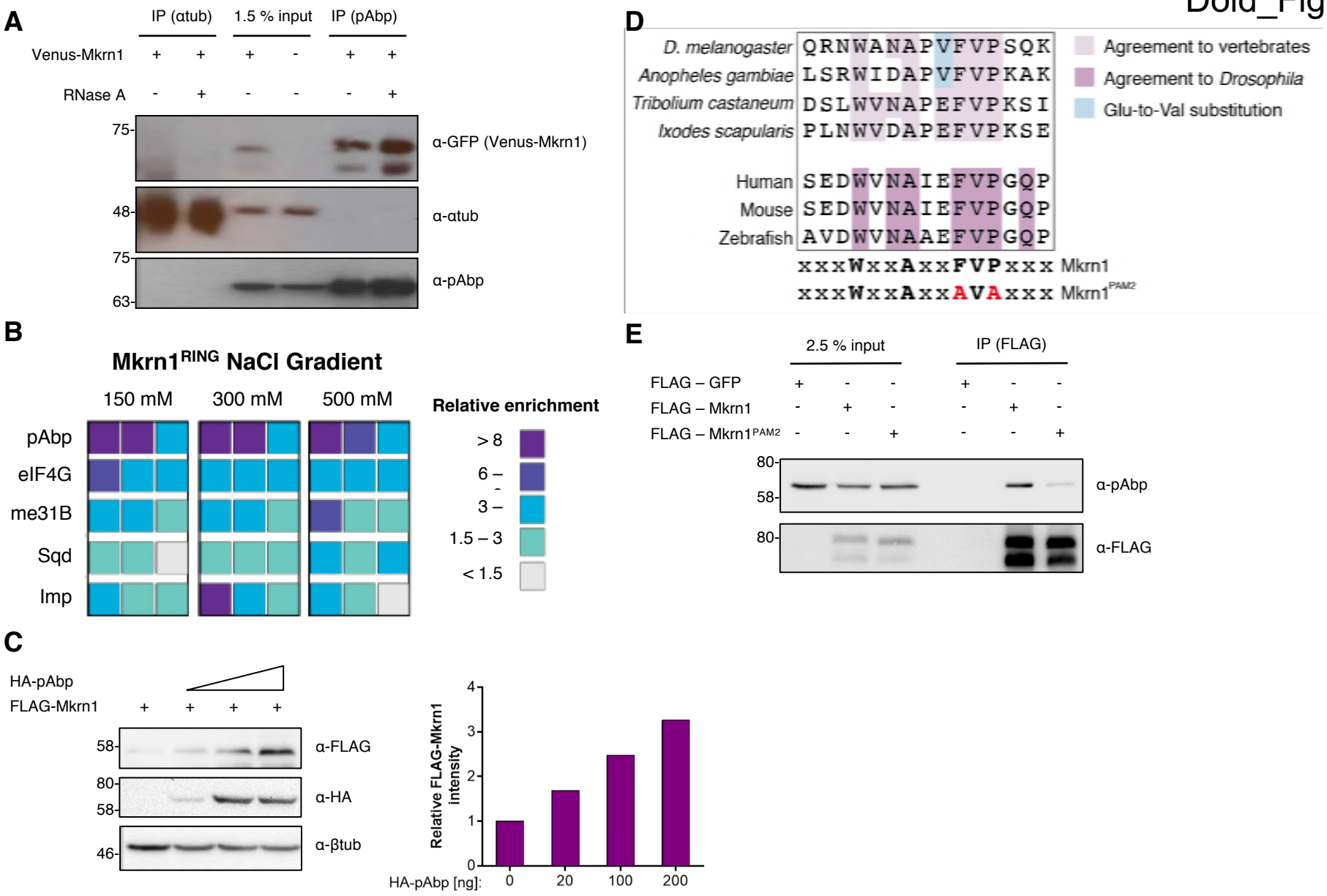
A
IP (αtub)
1.5 % input
IP (pAbp)
Venus-Mkrn1
RNase A
75-
48-
75-
63-
α-GFP (Venus-Mkrn1)
α-αtub
α-pAbp
B
Mkrn1RING NaCl Gradient
150 mM
300 mM
500 mM
pAbp
eIF4G
me31B
Sqd
Imp
Relative enrichment
> 8
6 –
3 –
1.5 – 3
< 1.5
C
HA-pAbp
FLAG-Mkrn1
58-
80-
58-
46-
α-FLAG
α-HA
α-βtub
Relative FLAG-Mkrn1 intensity
HA-pAbp [ng]:
0
20
100
200
D
D. melanogaster
Anopheles gambiae
Tribolium castaneum
Ixodes scapularis
Human
Mouse
Zebrafish
Agreement to vertebrates
Agreement to Drosophila
Glu-to-Val substitution
xxxWxxAxxFVPxxx Mkrn1
xxxWxxAxxAVAxxx Mkrn1PAM2
E
2.5 % input
IP (FLAG)
FLAG – GFP
FLAG – Mkrn1
FLAG – Mkrn1PAM2
80-
58-
80-
α-pAbp
α-FLAG

Dold_Fig6

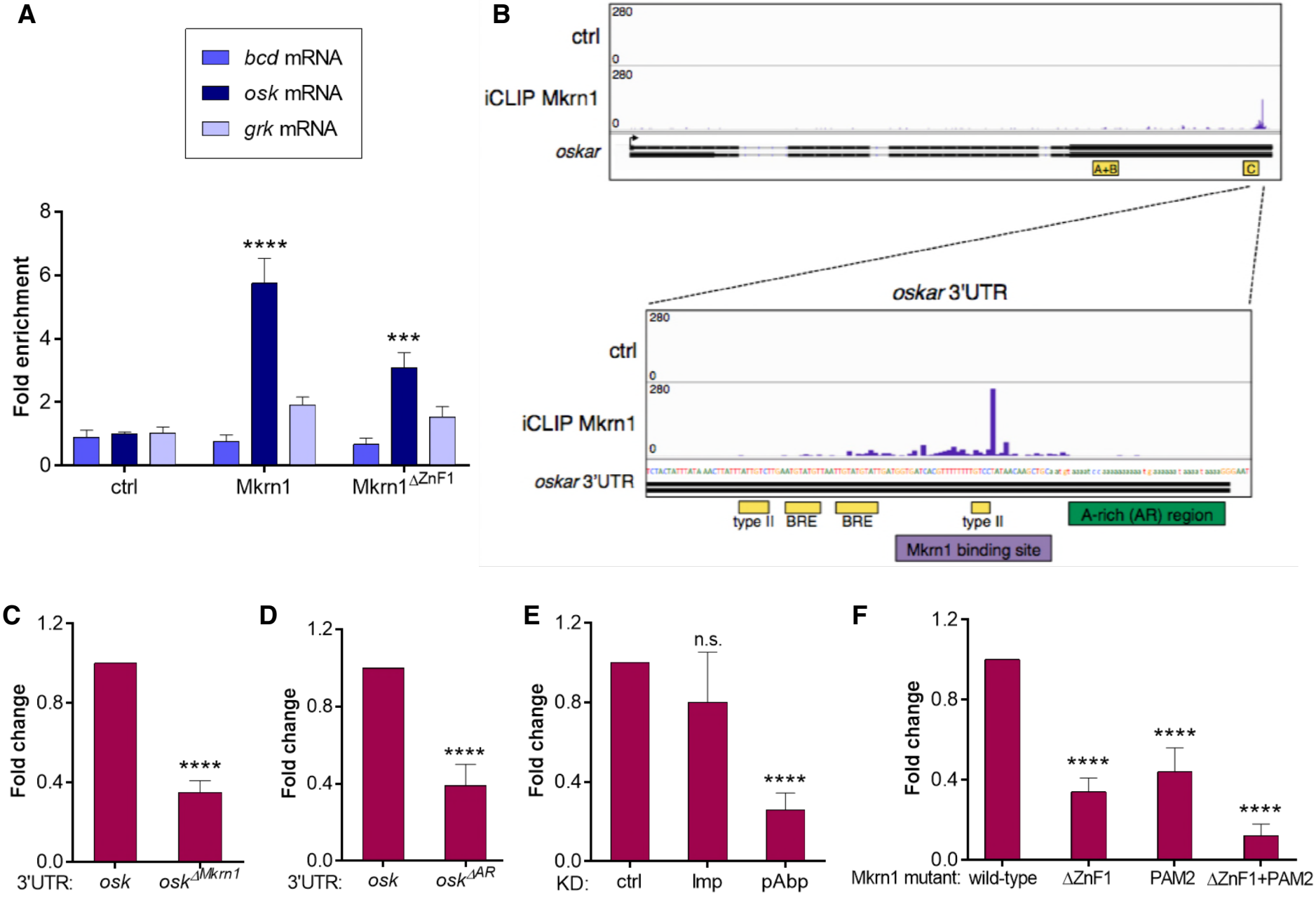
A
bcd mRNA
osk mRNA
grk mRNA
Fold enrichment
ctrl
Mkrn1
Mkrn1ΔZnF1
****
***
B
ctrl
iCLIP Mkrn1
oskar
A+B
C
oskar 3'UTR
type II
BRE
BRE
type II
A-rich (AR) region
Mkrn1 binding site
C
Fold change
3'UTR: osk
osk⊿Mkrn1
D
3'UTR: osk
osk⊿AR
E
n.s.
KD: ctrl
Imp
pAbp
F
Mkrn1 mutant: wild-type
ΔZnF1
PAM2
ΔZnF1+PAM2

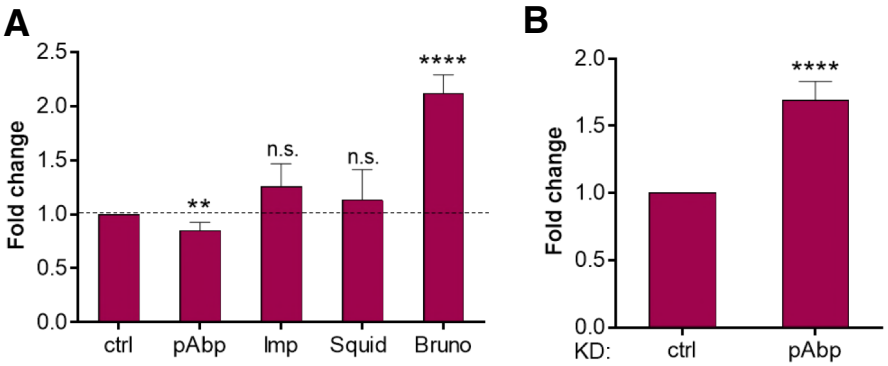
A
Fold change
2.5
2.0
1.5
1.0
0.5
0.0
**
n.s.
n.s.
****
ctrl
pAbp
Imp
Squid
Bruno
B
Fold change
2.0
1.5
1.0
0.5
0.0
****
KD:
ctrl
pAbp

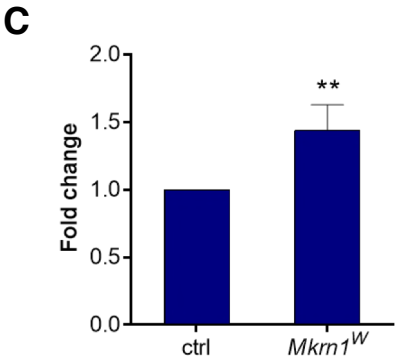
C
Fold change
2.0
1.5
1.0
0.5
0.0
**
ctrl
Mkrn1W

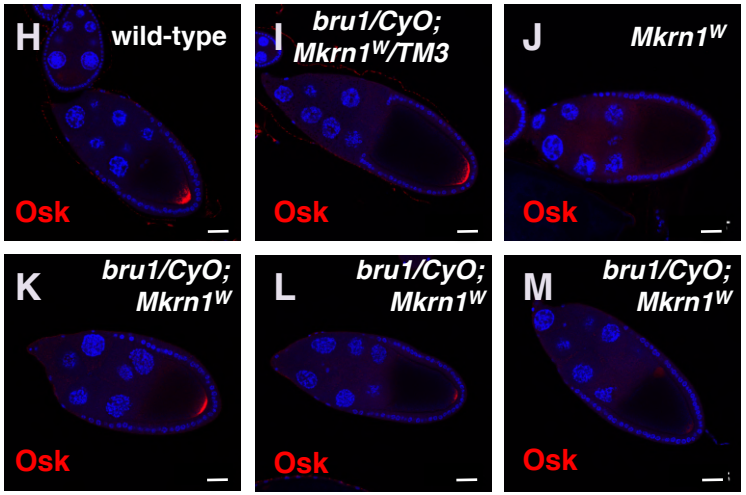
H
wild-type
Osk
I
bru1/CyO;
Mkrn1W/TM3
Osk
J
Mkrn1W
Osk
K
bru1/CyO;
Mkrn1W
Osk
L
bru1/CyO;
Mkrn1W
Osk
M
bru1/CyO;
Mkrn1W
Osk

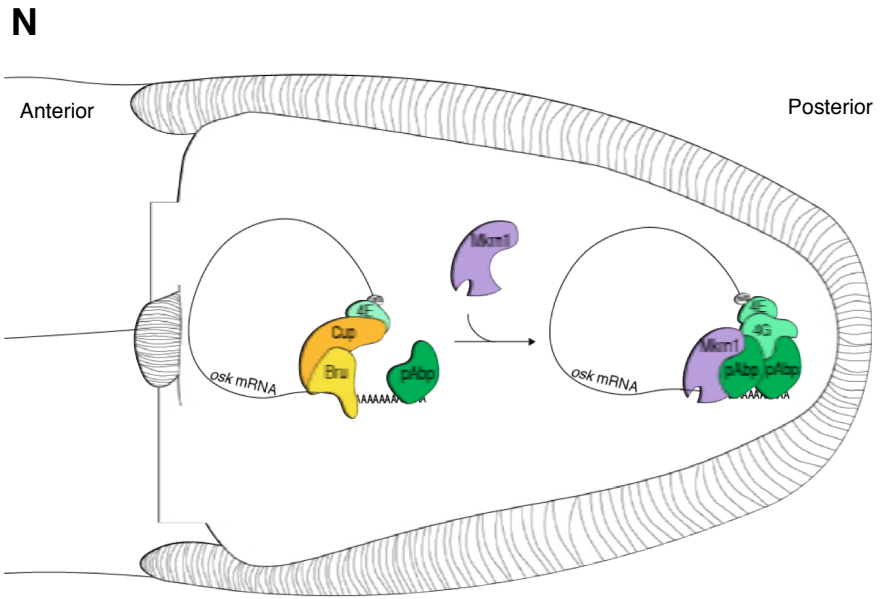
N
Anterior
Posterior
osk mRNA
4E
Cup
Bru
pAbp
Mkrn1
osk mRNA
4E
4G
Mkrn1
pAbp
pAbp

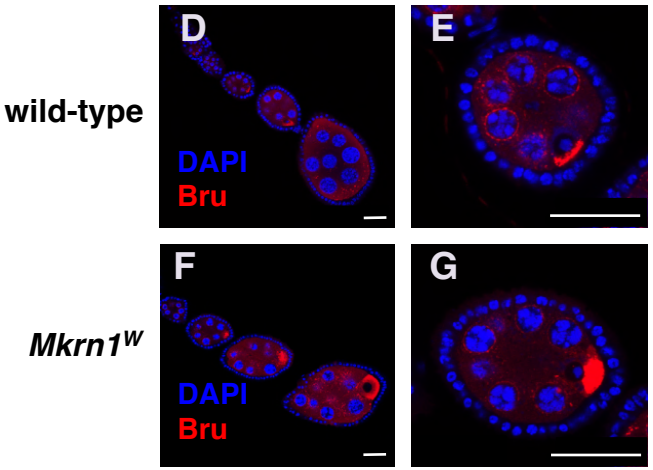
wild-type
D
DAPI
Bru
E
Mkrn1W
F
DAPI
Bru
G